Robust Deadbeat Predictive Direct Speed Control for PMSM With Dual Second-Order Sliding-Mode Disturbance Observers and Sensitivity Analysis

Shaobin Li, Yongxiang Xu, *Member, IEEE*, Wentao Zhang, and Jibin Zou, *Senior Member, IEEE*

***Abstract*—A novel robust deadbeat predictive direct speed control (RDP-DSC) method for permanent magnet synchronous motor is proposed to improve the speed control bandwidth and eliminate the conventional cascaded speed control structure. First, the basic DP-DSC method with one-step ahead time delay compensation is introduced briefly. Then, the control sensitivity analysis issue on the electrical and mechanical parameter mismatches, and external disturbance and inverter nonlinearity are inspirationally discussed. Further, based on the analysis above, a novel dual second-order sliding-mode disturbance observer (SOSMDO) structure is proposed for both current and speed disturbance suppression. The proposed RDP-DSC equipped with SOSMDO is presented with full control errors completely compensated. Meanwhile, the undesired chattering phenomenon caused by the switching function in the existing popular sliding-mode observers is eliminated by the proposed SOSMDO. Rich experiments are then performed, showing that the proposed method has strong enough robustness to various parameter mismatches and external disturbances while the system still holds the DSC methods' advantages, such as high response speed and satisfying bandwidth.**

***Index Terms*—Direct speed control (DSC), permanent magnet synchronous motor (PMSM), second-order sliding-mode disturbance observer (SOSMDO), sensitivity analysis.**

I. Introduction

PREDICTIVE control has become a hot issue in motor control fields because of its advantages, such as good dynamical performance, capability of dealing with multiinput multioutput systems, and easy constraints handling ability. Further, its combination with permanent magnet synchronous motor (PMSM) has shown great potential and is attracting increasing attention [1], [2].

Up till now, the most popular predictive control scheme in PMSM control area is predictive current control (PCC). On this scenario, the current controller is designed based on predictive control theory while a linear proportional–integral (PI) speed controller is typically utilized for speed control in the cascaded structure [3], [4]. The advanced current control performance can somewhat improve the system's performance. However, when it comes to the outer loop speed control, the dynamic performance is still tremendously limited by the double closed-loop cascaded control structure [5].

Recently, an emerging technique called predictive direct speed control (P-DSC) is proposed and widely studied, which eliminates the conventional cascaded PMSM speed control structure [6]. By eliminating the traditional cascaded structure, P-DSC not only inherits the merits of the predictive control algorithm but can also improve the system's bandwidth because the constraint of the outer loop slow dynamics is taken away [7]. Normally, P-DSC can be categorized into model predictive direct speed control (MP-DSC) [8], [9] and deadbeat predictive direct speed control (DP-DSC) [10], [11], [12], [13]. Based on the discrete PMSM model, MP-DSC optimizes a predefined cost function by evaluating all the available voltage vectors of the inverter [35]. For example, MP-DSC with an extended Kalman filter is used in a two-mass system driven by a PMSM in [8], and artificial neural networks are utilized for the selection of weighting factors in [9]. Even if no modulator is required, MP-DSC still has drawbacks, including large speed ripple, high calculation complexity, variable switching frequency, and painstaking weighing factor selection procedure [36].

Regarding the DP-DSC method, the idea is to generate the reference dq-axis voltages by the reference speed and d-axis reference current in a deadbeat manner, moving the motor's operating point precisely to the reference in the next moment. Afterwards, a modulator is required to interpret the signals to switching states before they are delivered to the inverter [26]. Compared with other MP-DSC methods, DP-DSC can enhance the speed control quality with less speed ripple, less calculation, fixed switching frequency, and faster control response [10]. In [28], a DSC method is designed by the deadbeat principle and a load torque observer (TO) is added to add robustness. Moreover, an enhanced predictive model and an exponential extended state observer are combined to realize deadbeat speed control [37]. Up till now, DP-DSC has not been well studied in the DSC field and has become a hot issue to be further developed.

However, similar to other model-based methods, the DP-DSC method relies highly on the precise modeling of the motor plant as well as load torque [14]. In fact, even if all the parameters

Manuscript received 22 October 2022; revised 20 January 2023 and 13 March 2023; accepted 10 April 2023. Date of publication 14 April 2023; date of current version 19 May 2023. Recommended for publication by Associate Editor A. M. Bazzi. *(Corresponding author: Jibin Zou.)*

The authors are with the School of Electrical Engineering and Automation, Harbin Institute of Technology, Harbin 150001, China (e-mail: flyingshaobin@gmail.com; xuyx@hit.edu.cn; zhang_wentaohit@163.com; zoujibin@hit.edu.cn).

Color versions of one or more figures in this article are available at https://doi.org/10.1109/TPEL.2023.3267172.

Digital Object Identifier 10.1109/TPEL.2023.3267172

are measured accurately offline, the motor parameters may largely change when PMSM operates under different conditions. For example, if the ambient temperature changes dramatically during operation, the actual flux linkage and resistance will deviate far away from nominal values. Consequently, this model mismatch will damage the transient tracking performance and result in steady-state speed tracking error, or in the worst case, system failure. In order to improve the robustness of DP-DSC, scholars have proposed various compensation methods, such as identification-based methods [15], [16], [17], augmented model methods [18], [19], and most importantly, the observer-based techniques [20], [21], [22], [23], [24], [25].

The parameter identification methods enhance the system's robustness by accurately identifying all motor parameters in the controller. In [15], a novel parameters identification method for the stator resistance and inductance is developed based on a reconstructed characteristic vector to achieve zero-steady-state error. In [16], an adaptive estimation law for unknown parameters is built with stability and robustness guaranteed. Besides in [17], stator inductance is extracted to improve the parameter robustness of predictive control system. However, identification-based compensation methods can only deal with parameter mismatches, while the disturbance rejection ability to varying parameters or unmodeled dynamics is poor.

Scholars also consider augmenting state-space model to endow the controller with robustness. For example, Wang [18] introduces the augmented model, where an integral action is brought in to eliminate steady-state error. In [19], an incremental model is applied for flux mismatch immunity control and the observer is incorporated to deal with other disturbances. These methods aim to augment the model to form an internal integrator for eliminating steady-state error. However, the dynamic performance cannot be guaranteed.

Recently, with the development of advanced control theory, observer-based control methods are designed to add certain robust to predictive controllers, such as Luenberger observers [20], Kalman filter [21], etc. Among all these observers, sliding-mode observer (SMO) has the advantage of really strong robustness. In [22], a sliding-model full parameter disturbances and load observer (FPLO) is put forward. Such an observer can simultaneously estimate electrical parameter disturbances, mechanical parameter disturbances, voltage reconstruction error, motor speed, and external load torque with the feasibility proved by experiments. What is more, an adaptive integral sliding-mode model predictive control is designed to improve robustness and reduce chattering [23]. In [24] and [25], super-twisting algorithm is used for disturbance estimation, and the results are then used in the main controller for disturbance rejection. In [7], a sliding term is added to the cost function to ensure robustness, but the resultant chattering is not negligible. Also, in [37], a unified high-order SMO is designed to increase the speed control robustness and current tracking accuracy.

In fact, the overall disturbance can be divided into the outer loop and inner loop disturbance in the DP-DSC control topology. The outer loop disturbance includes load torque, friction, and mechanical parameter mismatches, while the inner one consists of electrical parameter mismatches, inverter nonlinearity, and other unmodeled dynamics. Obviously, the features of both disturbances are different in terms of amplitude and change rate. Suppose only a single SMO is used for overall lumped disturbance estimation. In that case, the observer gains need tuning large enough to ensure convergence, which in turn brings in severe chattering and deteriorates the control performance. Resultantly, the optimal disturbance observation and speed control performance cannot be guaranteed. Hence, compared with the conventional single-observer-based methods in DSC, it is necessary to present a dual disturbance observer structure in which different gains are specially designed for the disturbances in either the inner or outer loop to ensure a perfect perturbation estimation and error suppression.

In this article, a novel robust deadbeat predictive direct speed control (RDP-DSC) method for surface-mounted PMSM (SPMSM) based on DP-DSC topology and the dual second-order sliding-mode disturbance observer (SOSMDO) structure is proposed. This method belongs to the general disturbance-observer-based control field. The novelties and main contributions can be summarized as follows:

1) First, a novel PMSM model is derived considering uncertainties, including both parameter mismatches and external disturbances, and a simple but effective DP-DSC controller is constructed in a deadbeat manner. The deadbeat control signal is directly generated from the PMSM equation considering one step ahead time delay compensation with hardly any computational complexity.
2) Further, considering various disturbance sources in the system, sensitivity analysis on how parameter mismatches, external disturbances, and inverter nonlinearity affect the speed tracking performance is quantitatively performed. Sensitivity analysis through discrete-time transfer function is put forward for the first time. And the influence on both steady-state and transient-state control behavior can be clearly concluded, which serves as a general guideline for disturbance observer design and tuning.
3) A novel RDP-DSC method is put forward for both current and speed error suppression to enhance the robustness of the DP-DSC controller. The proposed dual SOSMDO structure can decouple the inner and outer disturbance for individual estimation, which means that each observer gain can be specially designed considering different amplitudes and change rates of the inner and outer loop disturbance. The dual observer structure along with the second-order SMO design makes the RDP-DSC have strong superiority over other conventional disturbance observer based, especially SMO based, DSC methods in terms of lower speed ripple, and stronger disturbance rejection ability.

The rest of this article is organized as follows. The mathematical model of PMSM with disturbance is formulated and the conventional DP-DSC controller design is introduced in Section II. Then, Section III conducts the sensitivity analysis against parameter mismatches, inverter nonlinearity, and external disturbance. Section IV presents the proposed dual SOSMDO structure and the RDP-DSC method. In Section V, the effectiveness of the proposed method is verified by a series of experiments.

Finally, Section VI concludes this article and discusses the future work.

II. Mathematical Model of PMSM and Conventional DP-DSC Method

The PMSM mathematical model, including parameter mismatches and external disturbances, is formulated in this section. Then, a one-step delay compensation algorithm in predictive control is introduced. And the conventional DP-DSC is briefly introduced to realize deadbeat speed control.

A. PMSM Mathematical Model

In the synchronous rotating frame (dq-frame), the electrical and mechanical dynamics of an SPMSM can be constructed mathematically with nominal parameters (usually measured offline and used in the controller) as follows:

$$\begin{cases} \frac{di_d}{dt} = \frac{1}{L_0}u_d - \frac{R_0}{L_0}i_d + \omega_e i_q + d_d \\ \frac{di_q}{dt} = \frac{1}{L_0}u_q - \frac{R_0}{L_0}i_q - \omega_e i_d - \frac{\psi_{f0}\omega_e}{L_0} + d_q \\ \frac{d\omega_m}{dt} = \frac{3p\psi_{f0}i_q}{2J_0} + d_\omega \end{cases} \tag{1}$$

where u_d and u_q are dq-axis voltages; i_d and i_q are dq-axis currents; L_0 is the dq-axis inductance; R_0 is the stator resistance; ψ_{f0} is the permanent magnet flux linkage; ω_e and ω_m mean the electrical and mechanical angular velocity, respectively; p means the pole pairs; J_0 is the inertia; d_d and d_q are lumped disturbance for current equation; and d_ω is the disturbance for speed dynamics. Besides, parameters with subscript "0" denote the nominal value used in the controller.

Further, the disturbance can be further extended as follows including parameter mismatches, external load torque, and unmodeled dynamics into consideration:

$$\begin{cases} d_d = \left(\frac{1}{L} - \frac{1}{L_0}\right)u_d - \left(\frac{R}{L} - \frac{R_0}{L_0}\right)i_d + \varepsilon_d \\ d_q = \left(\frac{1}{L} - \frac{1}{L_0}\right)u_q - \left(\frac{R}{L} - \frac{R_0}{L_0}\right)i_q - \left(\frac{\psi_f}{L} - \frac{\psi_{f0}}{L_0}\right)\omega_e + \varepsilon_q \\ d_\omega = -\frac{3p\psi_{f0}i_q}{2J_0} + \frac{3p\psi_f i_q}{2J} - \frac{B}{J}\omega_m - \frac{T_L + T_f}{J} \end{cases} \tag{2}$$

where ε_d and ε_q mean the unmodeled dynamics, such as the inverter nonlinearity; B is the viscous damping; T_L and T_f are the load torque and friction, respectively; and other parameters without subscript "0" denote the real motor parameters.

B. One-Step Delay Compensation

Before constructing DP-DSC controller, time delay effect in a real PMSM digital control system should be considered and compensated by a one-step ahead prediction method [26]. That is, DP-DSC output $\boldsymbol{u}_{dq0}(k+1)$ for $t = k+1$ should be calculated one step ahead at $t = k$ moment so that this signal can be implemented to the inverter at $t = k+1$ without delay. Note that the bold font represents vector variables in the whole paper, while $\boldsymbol{u}_{dq0}(k+1)$ is comprised of $u_{d0}(k+1)$ and $u_{q0}(k+1)$. If all the disturbances are ignored, the ideal control voltage can be obtained by discretization of (1) according to [27] as follows:

$$\begin{cases} u_{q0}(k+1) = \frac{L_0}{T}\cdot i_q(k+2) - \frac{L_0}{T}\cdot\left(1 - \frac{TR_0}{L_0}\right)\cdot \hat{i}_{q0}(k+1) \\ \quad + (L_0\hat{i}_{d0}(k+1) + \psi_{f0})\omega_e(k) \\ u_{d0}(k+1) = \frac{L_0}{T}i_d(k+2) - \frac{L_0}{T}\left(1 - \frac{TR_0}{L_0}\right)\hat{i}_{d0}(k+1) \\ \quad - L_0\omega_e(k)\hat{i}_{q0}(k+1) \end{cases} \tag{3}$$

where T is the sampling time and the values annotated by k are sampled at the kth sampling instant. Note that $\omega_e(k)$ is used to replace $\omega_e(k+1)$ because the motor speed can be regarded as unchanged in the adjacent control periods [26].

In the equation above, the future dq-axis currents $\hat{\boldsymbol{i}}_{dq0}(k+1)$ at time $t = k+1$ cannot be measured directly at $t = k$. Therefore, prediction is needed based on $t = k$ measurement $\boldsymbol{i}_{dq}(k)$ and the electrical mathematical equation in (1)

$$\begin{cases} \hat{i}_{q0}(k+1) = \left(1 - \frac{TR_0}{L_0}\right)\cdot i_q(k) - T\omega_e(k)i_d(k) \\ \quad - \frac{T\omega_e(k)\psi_{f0}}{L_0} + \frac{T}{L_0}u_q(k) \\ \hat{i}_{d0}(k+1) = \left(1 - \frac{TR_0}{L_0}\right)\cdot i_d(k) + T\omega_e(k)i_q(k) + \frac{T}{L_0}u_d(k). \end{cases} \tag{4}$$

According to the deadbeat principle, the predicted current is typically selected as the reference current so that PMSM will track this reference current at the next moment. Hence, $\boldsymbol{i}_{dq}(k+2)$ in (3) can be viewed as the desired current value to be exactly tracked at $t = k+2$. In other words, $\boldsymbol{i}_{dq}(k+2)$ serves as the reference value for $t = k$. Since the d-axis current is always controlled to be zero for SPMSM, $i_d^* = i_d(k+2) = 0$ can be used. When it comes to $i_q(k+2)$, it is treated as an intermediate variable in the DP-DSC controller and will be further illustrated in the following section.

C. DP-DSC Controller Design

To achieve DSC performance, the current and speed loops in the conventional cascaded control topology are merged into one single loop to form a cascaded-free structure. Hence, the overall voltage control signal can be directly generated based on the speed reference value.

The discretized mechanical equation can be written as (5) by forward Euler expansion regardless of disturbances according to [22]. The sampling interval of the speed dynamics is defined as $T_p = T\xi$, where ξ is a positive integer larger than 1 (typically 5 to 10) to prevent the coupling of speed control and current control on each other [28]. This statement is reasonable because the mechanical dynamics is usually much slower than the current one in the motor control system, and the speed sampling interval is denoted by n. Hence, during $t = n$ and $t = n+1$, the q-axis current will be regulated several times to track the same reference $i_q^* = i_q(n)$. Since $i_q(k+2)$ is the reference value to be followed for the deadbeat controller considering delay compensation at $t = k$, $i_q(k+2)$ is used instead of $i_q(n)$ as follows for expression simplicity:

$$\omega_m(n+1) = \omega_m(n) + \frac{3p\psi_{f0}i_q(k+2)}{2J_0}T_p \tag{5}$$

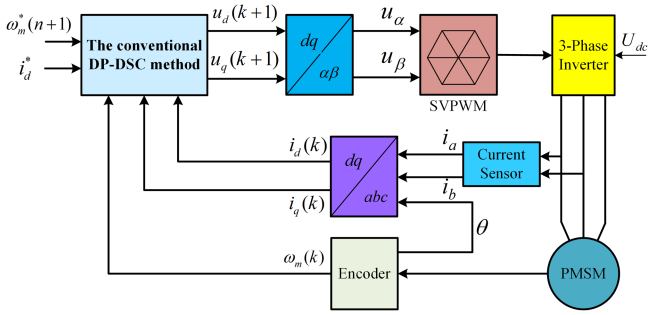

Fig. 1. Schematic diagram of the PMSM control system based on the conventional DP-DSC method.

where $\omega_m(n)$ and $\omega_m(n+1)$ mean the speed value at $t=n$ and $t=n+1$, respectively, while n denotes the speed sampling instant.

Obviously, the intermediate current reference $i_q(k+2)$ can be further written as (6a) to achieve deadbeat speed tracking performance. And from the analysis above, $i_q(k+2)$ can also be interpreted as the q-axis current reference value i_q^*

$$i_q^* = i_q(k+2) = \frac{2J_0\left(-\omega_m(n)+\omega_m^*(n+1)\right)}{3p\psi_{f0}T\xi} \tag{6a}$$

where the values with asterisks mean the reference values. And in the ideal case, $\omega_m^*(n+1)$ can be exactly tracked at $t=n+1$ without any error. In fact, the amplitude of the q-axis current reference may not exceed the control system's current limitation. That is, a clamp is needed. Hence, the modified q-axis current reference should be constrained as follows:

$$i_q^* = Sat\left(\frac{2J_0\left(-\omega_m(n)+\omega_m^*(n+1)\right)}{3p\psi_{f0}T\xi}\right) \tag{6b}$$

where "*Sat*" means the saturation function constrained by the maximum allowed q-axis current amplitude $I_{q\max}$.

By plugging in (4) and (6b) into (3), the control voltage of the DP-DSC controller can be calculated as (7). This voltage is then exerted on the modulator for switching states calculation

$$\begin{cases} u_{q0}(k+1) = \frac{L_0}{T}\cdot Sat\left(\frac{2J_0(-\omega_m(n)+\omega_m^*(n+1))}{3p\psi_{f0}T\xi}\right) \\ \quad +A_{q0}(k+1) \\ u_{d0}(k+1) = A_{d0}(k+1) \end{cases} \tag{7}$$

where $A_{d0}(k+1)$ and $A_{q0}(k+1)$ are expanded in detail at the bottom of this page, and the overall DP-DSC method diagram can be depicted in Fig. 1.

III. Sensitivity Analysis on Parameter Mismatch and External Disturbance

In order to obtain ideal deadbeat speed tracking performance, the control voltage must be accurately calculated assuming that the nominal and the actual model are identically the same. However, parameter mismatches (stator resistance R_0, stator inductance L_0, flux-linkage ψ_{f0}, and inertia J), inverter nonlinearity, as well as other external disturbances (such as load torque T_L and friction T_f) are unavoidable in reality. Therefore, it is necessary to quantitatively evaluate to what extent the aforementioned disturbances can affect the speed control performance. This section performs sensitivity analysis to form a guideline for further observer design and gain tuning.

A. Influence of Flux Linkage Mismatch

In reality, the permanent magnet flux linkage is prone to be affected by the ambient temperature during motor operation. For example, a 20% flux reduction may occur per 100 °C ambient temperature rise for ferrite-based magnet [32]. The flux linkage error is defined as the real value minus the nominal value $\Delta\psi_f = \psi_f - \psi_{f0}$. Suppose that the inverter is ideal and the calculated voltage signal in (7) can be exerted on the real motor without any loss. When analyzing flux linkage mismatch, all the other disturbances are set as zero. If the control signal in (7) is brought into the motor (1) and all the nominal values in (1) are replaced by real motor values, the resultant rotor speed can be simplified as follows when higher order terms of the control period T (third-order or higher) are omitted:

$$\begin{aligned}\omega_m(n+1) = \omega_m^*(n+1) - \frac{3\Delta\psi_f p^2T^2\xi\psi_f}{J_0L_0}\omega_m(n) \\ - \frac{\Delta\psi_f\left(\omega_m(n)-\omega_m^*(n+1)\right)}{\psi_{f0}}.\end{aligned} \tag{8}$$

Obviously, the flux linkage mismatch will slow down the dynamic tracking performance because the terms containing $\Delta\psi_f$ and rotor speed may force the velocity to deviate from the reference. Discrete-time control theory analysis can also testify to this conclusion. The transfer function between the speed feedback and reference can be written as follows by applying z-transformation to (8):

$$H_{\psi_f}(z) = \frac{\omega_m(z)}{\omega_m^*(z)} = \frac{\psi_f}{\psi_{f0}}\cdot\frac{z}{z+\left(\frac{3\Delta\psi_f p^2T^2\xi\psi_f}{J_0L_0}+\frac{\Delta\psi_f}{\psi_{f0}}\right)}. \tag{9}$$

It is known that the deadbeat tracking performance requires the system's closed-loop pole to be located exactly at the origin. However, with flux linkage error, the transfer function has only a single pole at $z=-(\frac{3\Delta\psi_f p^2T^2\xi\psi_f}{J_0L_0}+\frac{\Delta\psi_f}{\psi_{f0}})$. According to the control theory, the system exhibits overdamping feature if the pole resides on the positive real axis, while the system oscillates when the pole lies in the negative part. In both cases, the settling time will be prolonged under flux mismatch, and the dynamic performance will be deteriorated. Apparently, when the flux mismatch grows closer to somewhere near ψ_{f0} or $-\psi_{f0}$, the absolute value of this pole locates outside the unit circle, and the system becomes unstable. Hence, it can be concluded that the stability region for flux linkage mismatch $\Delta\psi_f$ is a subset of the range $(-\psi_{f0}, \psi_{f0})$, unnumbered equation shown at the bottom of the next page.

As for the influence of flux linkage mismatch on the steady-state performance, assume that $\omega_m(n+1)=\omega_m(n)$ and then (10) can be derived from (8). It can be seen that the actual speed will be bigger than the reference if $\Delta\psi_f$ is smaller than 0 and vice versa. Therefore, if not compensated, flux linkage error will

bring in unacceptable steady-state error

$$\omega_m(n+1)=\frac{J_0L_0}{J_0L_0+3\Delta\psi_f p^2T^2\xi\psi_{f_0}}\omega_m^*(n+1). \quad (10)$$

B. Influence of Inertia Mismatch

Typically, the rotor inertia is hard to be accurately measured, and its value may change during operation. If we denote $\Delta J = J - J_0$, the actual speed obtained by the DP-DSC method can be deduced as (11) following the similar derivation procedure in Section A. Obviously, it can be seen that the inertia mismatch will not introduce any steady-state error. The reason is that if $\omega_m(n+1)=\omega_m(n)$ holds in the steady state, the equality $\omega_m(n+1)=\omega_m^*(n+1)$ can be obtained from the speed response expression under inertia mismatch

$$\omega_m(n+1)=\frac{\Delta J}{J_0+\Delta J}\omega_m(n)+\frac{J_0}{J_0+\Delta J}\omega_m^*(n+1). \quad (11)$$

However, when it comes to the transient performance, too large inertia deviation will deteriorate the system severely and may even cause instability. *Z*-transformation is applied to (11) to analyze this issue, and the discrete transfer function between speed reference and response can be obtained as

$$H_L(z)=\frac{\omega_m(z)}{\omega_m^*(z)}=\frac{zJ_0}{z(J_0+\Delta J)-\Delta J}. \quad (12)$$

Apparently, this transfer function has a single pole located at $z=\Delta J/(J_0+\Delta J)$, which means that inertia mismatch handicaps the ideal deadbeat control performance. What is more, all the poles of $H_L(z)$ are required to locate within the unit circle $|z|<1$ so that the stability of the entire system can be ensured [29]. In this case, the stability region of the nominal inertia can be calculated as follows, which means that if the absolute value of the inertia mismatch is greater than the real value, the system diverges and becomes unstable:

$$0<J_0<2J. \quad (13)$$

C. Influence of Resistance Mismatch

The variation of the resistance may come from the motor temperature change. For example, the stator winding resistance increases as the ambient temperature rises [34]. If we denote $\Delta R = R - R_0$ as the real value minus the nominal one and follow the analysis procedure above, the real motor speed under the conventional DP-DSC method can be depicted as

$$\omega_m(n+1)=\omega_m^*(n+1)+o\left(T^2\right) \quad (14)$$

where $o(T^2)$ means the terms containing the order equal to or higher than T^2.

From (14), the tiny speed tracking error is negligible, and the resistance mismatch hardly affects the system's performance both in transient and steady state. Even so, the nominal resistance value should still be as accurate as possible.

D. Influence of Inductance Mismatch

In reality, accurate measurement of stator inductance is quite challenging, and inductance mismatch is prone to happen in real controllers. In this case, the difference between the nominal and real inductance values is designated as $\Delta L = L - L_0$. Further, the corresponding motor speed under (7) is shown as follows:

$$\omega_m(n+1)=\frac{\Delta L}{L_0+\Delta L}\omega_m(n)+\frac{L_0}{L_0+\Delta L}\omega_m^*(n+1)+\frac{3pi_q(k)\psi_{f0}T\Delta L}{2J_0(L_0+\Delta L)}. \quad (15)$$

The analysis of the transient-state performance is similar to the one in the inertia mismatch case with the deviated closed-loop pole locating at $z=\Delta L/(L_0+\Delta L)$. Similarly, the inductance mismatch will deteriorate the transient tracking performance, and a system failure will happen if the mismatch value ΔL is larger than L.

As for the steady-state tracking performance, the following equation can be deduced by the assumption that $\omega_m(n+1)=\omega_m(n)$:

$$\omega_m(n+1)=\omega_m^*(n+1)+\frac{3pi_q(k)\psi_{f0}T}{2J_0}\cdot\frac{\Delta L}{L_0}. \quad (16)$$

It is seen that the steady-state error grows proportionally with ΔL when the load torque is unchanged. However, the real motor speed may not deviate from the reference much because the error expression contains a sampling period T term, which is a relatively small constant.

E. Influence of External Disturbances

The external disturbance is represented by the d_ω term in (1), which mainly includes unexpected torque dynamics consisting of viscous damping, load torque, friction, etc. Considering this, the influence of d_ω can be deduced as (17) and it can be regarded as some deviation between the speed feedback and reference in the steady state. Also, it is evident that transient-state tracking performance is almost unaffected

$$\omega_m(n+1)=\zeta Td_\omega+\omega_m^*(n+1). \quad (17)$$

F. Influence of Inverter Nonlinearity

The inverter nonlinearity influence is generally composed of the dead-time effect as well as the diode and IGBT forward

$$\begin{cases} A_{q0}(k+1)=\frac{L_0}{T}\left(\begin{array}{l}\frac{T\psi_{f0}\omega(k)}{L_0}+T\omega(k)\left(i_d(k)\cdot\left(1-\frac{R_0T}{L_0}\right)+\frac{Tu_d(k)}{L_0}+T\omega(k)i_q(k)\right)\\ -\left(1-\frac{R_0T}{L_0}\right)\left(i_q(k)\left(1-\frac{R_0T}{L_0}\right)+\frac{Tu_q(k)}{L_0}-i_d(k)T\omega(k)-\frac{T\psi_{f0}\omega(k)}{L_0}\right)\end{array}\right)\\ A_{d0}(k+1)=2R_0i_d(k)-(\frac{R_0^2T}{L_0}+\frac{L_0}{T})i_d(k)+(\frac{R_0T}{L_0}-1-T\omega(k))u_d(k)+2i_q(k)\omega(k)(R_0T-L_0)\\ \quad +T\omega^2(k)(L_0i_d(k)+\psi_{f0}).\end{cases}$$

voltage drop. These undesired elements will cause a 6*k*th-order voltage distortion between the calculated control voltage and the real value delivered to the PMSM [39]. Consequently, the distorted voltage will produce a dc component as well as 6*k*th harmonics in the *dq*-axis currents of the synchronous reference frame, which can be modeled as follows [40]:

$$\begin{cases} i_{ds}^{\text{Dead}} = \sum_{k=1}^{\infty} i_{dk}^{\text{Dead}} \sin(6k\omega_e t + \phi_{6k}) \\ i_{qs}^{\text{Dead}} = i_{q0}^{\text{Dead}} + \sum_{k=1}^{\infty} i_{qk}^{\text{Dead}} \cos(6k\omega_e t + \phi_{6k}) \end{cases} \tag{18}$$

where i_{ds}^{Dead} and i_{qs}^{Dead} are the distorted *dq*-axis currents; i_{q0}^{Dead} and i_{qk}^{Dead} represent the amplitude of *q*-axis dc current component and 6*k*th-order harmonics, respectively; i_{dk}^{Dead} means the amplitude of *d*-axis 6*k*th-order harmonics; and ϕ_{6k} means the corresponding phase angle.

Since the current harmonics in the *d*-axis will not contribute to the torque performance, the analysis mainly focuses on the behavior of the *q*-axis current. Obviously, the influence of inverter nonlinearity can be regarded as an oscillating torque and can be deduced as (19) similar to subsection E. This effect will not only introduce certain steady-state tracking errors between the speed feedback and reference, but the undesired 6*k*th-order speed ripple will also occur in the speed response, which is unacceptable in high-performance speed control systems

$$\omega_m(n+1) = \zeta T \cdot \frac{3p\psi_f}{2J} \cdot i_{qs}^{\text{Dead}} + \omega_m^*(n+1). \tag{19}$$

To conclude, the conventional DP-DSC method holds hardly any robustness against parameter mismatches and other perturbations, which means that the ideal deadbeat speed control performance cannot be achieved in most cases in reality. Hence, developing a disturbance compensation scheme based on the proposed sensitivity analysis results is reasonably necessary to make the DP-DSC robust for real applications.

IV. Proposed RDP-DSC Method

This section proposes a novel RDP-DSC method with a dual SOSMDO-based compensation scheme. The error for current prediction, *q*-axis current reference generation, and voltage calculation can be suppressed simultaneously. Thus, the robustness of conventional DP-DSC is strongly improved, while the undesired chattering behavior from the conventional SMO is removed by the advanced SOSMDO.

A. Error Decomposition and Formulation

According to the DP-DSC voltage generation (7), three main aspects of disturbances in the design procedure should be compensated. First, the electrical parameter mismatches and other unmodeled dynamics in the motor current equation will lead to an inaccurate future current prediction. Compared with (4), the future current prediction error can be denoted as $\boldsymbol{d}_{dq}(k)$ as follows, where $\hat{\boldsymbol{i}}_{dq}(k+1)$ means the accurate current prediction value:

$$\begin{cases} \hat{i}_d(k+1) = \hat{i}_{d0}(k+1) + Td_d(k) \\ \hat{i}_q(k+1) = \hat{i}_{q0}(k+1) + Td_q(k). \end{cases} \tag{20}$$

Second, assume that we have already acquired an accurate $t = k+1$ current prediction value. Another aspect lies in the control voltage generation process where unknown disturbance $\boldsymbol{d}_{dq}(k+1)$ may deviate the calculated voltage in (7) from the value needed in practice as (21). Here, (21) is also obtained from (1) with all the disturbances considered. This deviation hinders the deadbeat speed control performance

$$\begin{cases} u_d(k+1) = \frac{L_0}{T} \cdot i_d^* - \frac{L_0}{T}\left(1 - \frac{TR_0}{L_0}\right) \cdot \hat{i}_d(k+1) \\ \quad -\omega_e(k) L_0 \hat{i}_q(k+1) - L_0 d_d(k+1) \\ u_q(k+1) = \frac{L_0}{T} \cdot i_q(k+2) - \frac{L_0}{T} \cdot \left(1 - \frac{TR_0}{L_0}\right) \cdot \hat{i}_q(k+1) \\ \quad +(L_0 \hat{i}_d(k+1) + \psi_{f0})\omega_e(k) - L_0 d_q(k+1). \end{cases} \tag{21}$$

What is more, perturbations in the mechanical equation, such as the inertia mismatch and unknown load torque, will influence the intermediate *q*-axis reference current i_q^* calculation. The generation of i_q^* in this case should consider $d_\omega(k)$ on the basis of (6a), and the updated equation goes as (22). The neglected term $d_\omega(k)$ will unavoidably slow down the speed tracking performance and cause steady-state error

$$i_q^* = i_q(k+2) = \frac{2J_0}{3p\psi_{f0}\xi}\left(\frac{-\omega_m(n) + \omega_m^*(n+1)}{T} - d_\omega(k)\right). \tag{22}$$

To conclude, three types of disturbances are decomposed and formulated, respectively. Obviously, a robust design is needed for the conventional DP-DSC method. A feasible but straightforward solution is to compensate for each disturbance, respectively, by independent disturbance observers, and this novel thought is discussed in detail in the following section.

B. Observer Design

A novel dual SOSMDO structure is designed in order to compensate for all the aforementioned disturbances. In this topology, multiple advanced SOSMDO are designed based on super-twisting algorithm theory, and they are used separately for both electrical disturbance and mechanical disturbance estimation. One main advantage is that each observer gain can be individually tuned considering different features of inner current loop disturbance and outer speed loop disturbance.

First, an inner SOSMDO observer is constructed for the current prediction correction and the voltage generation error observation. The inner loop observers can be built as follows in compact form based on [30], and the observation results can be further used to compensate for the negative influence of current loop disturbances:

$$\begin{cases} \dot{\hat{\boldsymbol{i}}}_{dq} = \mathbf{A}\boldsymbol{i}_{dq} + \mathbf{B}\boldsymbol{u}_{dq} + \mathbf{H} + \hat{\boldsymbol{d}}_{dq} - \boldsymbol{\lambda}_{dq}\sqrt{|\boldsymbol{e}_{dq}|}\,sign(\boldsymbol{e}_{dq}) \\ \dot{\hat{\boldsymbol{d}}}_{dq} = -\boldsymbol{\alpha}_{dq}\,sign(\boldsymbol{e}_{dq}) \end{cases} \tag{23}$$

where $\boldsymbol{\alpha} = \begin{pmatrix} -R_0/L_0 & \omega_e \\ -\omega_e & -R_0/L_0 \end{pmatrix}$, $\mathbf{B} = \begin{pmatrix} 1/L_0 & 0 \\ 0 & 1/L_0 \end{pmatrix}$, $\hat{\boldsymbol{d}}_{dq} = \begin{pmatrix} \hat{d}_d \\ \hat{d}_q \end{pmatrix}$ $\mathbf{H} = \begin{pmatrix} 0 \\ -\psi_{f0}\omega_e/L_0 \end{pmatrix}$, $\boldsymbol{i}_{dq} = \begin{pmatrix} i_d \\ i_q \end{pmatrix}$, $\boldsymbol{u}_{dq} =$

$\begin{pmatrix} u_d \\ u_q \end{pmatrix}$, $\hat{\boldsymbol{i}}_{dq} = \begin{pmatrix} \hat{i}_{dq} & \hat{i}_q \end{pmatrix}^T$, $\boldsymbol{\lambda}_{dq}$, and $\boldsymbol{\alpha}_{dq}$ are observer gains to be tuned, $\boldsymbol{e}_{dq} = \hat{\boldsymbol{i}}_{dq} - \boldsymbol{i}_{dq}$ means the current observation error, and parameters denoted with "hat" are estimated values.

Obviously, the second-order sliding mode principle allows the "sign" function that results in chattering to hide inside an integral action, which contributes to eliminating the chattering phenomenon in essence. The convergence property of the proposed observer can be analyzed by the error equation. Since dq-axis current loops in the PMSM control system hold similar dynamics, we take q-axis loop observer behavior for illustration. Combining (1) and (23), the corresponding error equation can be written as

$$\begin{cases} \dot{e}_q = -\lambda_q \sqrt{|e_q|} sign(e_q) + e_{q\_\text{error}} \\ \dot{e}_{q\_error} = -\alpha_q sign(e_q) - \xi_q \end{cases} \tag{24}$$

where the q-axis disturbance observation error is $e_{q\_\text{error}} = \hat{d}_q - d_q$ and $|\dot{d}_q| = \xi_q$ represents the amplitude of the time derivative of the q-axis current loop disturbance.

In reality, it is reasonable to assume that the time derivative of the disturbance $\dot{d}_q$ has an upper bound η_q [26], which can be denoted by $|\dot{d}_q| = \xi_q < \eta_q$. Clearly, the condition above is a relaxation of the disturbance constraint and is suitable for more general cases than other observer-based methods that restrict the disturbance amplitude. Once the error (24) has been obtained, a family of strict Lyapunov functions can be selected for such systems as long as condition $|\dot{d}_q| = \xi_q < \eta_q$ holds [30]. Further, the finite-time convergence property can be proved mathematically and the detailed proof can be found in [33], which is not the main focus of this article. In this case, the observation errors e_{q_error} and e_q hold the finite-time convergence property if coefficients λ_q and α_q are properly chosen. Typically, dq-axis current loop disturbance observer gains are usually chosen as $\boldsymbol{\lambda}_{dq} = 1.5\sqrt{\boldsymbol{\eta}_{dq}}$, $\boldsymbol{\alpha}_{dq} = 1.1\boldsymbol{\eta}_{dq}$ for a good compromise between fast convergence and high observation accuracy [30], [31]. Consequently, both d_q and d_d can be precisely estimated by the inner SOSMDO observer and then used for accurate control signal generation.

Further, an outer SOSMDO observer is built for mechanical disturbance d_ω estimation to obtain an accurate intermediate reference current without bias. Similarly, in the PMSM system, it is also reasonable to find an upper bound η_q for the speed loop disturbance $|\dot{d}_\omega| < \eta_\omega$, and the corresponding observer can be designed as follows following a similar procedure:

$$\begin{cases} \dot{\hat{\omega}}_m = \frac{3p\psi_{f0} i_q}{2J_0} - \lambda_\omega \sqrt{|e_\omega|} sign(e_\omega) + \hat{d}_\omega \\ \dot{\hat{d}}_\omega = -\alpha_\omega sign(e_\omega) \end{cases} \tag{25}$$

where the speed disturbance observation error is $e_\omega = \hat{\omega}_m - \omega_m$ and $\hat{d}_\omega$ means estimation value.

The convergence feature of (25) is identical to the analysis above and $\lambda_\omega = 1.5\sqrt{\eta_\omega}$, $\alpha_\omega = 1.1\eta_\omega$ are chosen accordingly. Consequently, the inner and outer SOSMDO can accurately compensate for the overall disturbances, which is the key part of the proposed RDP-DSC method.

When selecting the observer gains η_{dq} and η_ω, the tuning is a tradeoff between the anti-disturbance property and the undesired chattering phenomenon in the response. First, large enough values covering the disturbance upper bound should be chosen for convergence while enough margin should be left for unexpected disturbance change. Note that the larger the observer gains are, the stronger anti-disturbance ability is endowed to the system because the tolerable varying rate of the disturbance is higher. Once the convergence is guaranteed, engineers can adjust the upper bounds based on the actual response performance. Either increase η_{dq} and η_ω for a stronger anti-disturbance ability or decrease them for less chattering. Meanwhile, even if the chattering caused by the "sign" function is significantly attenuated by an integral action in the proposed SOSMDO, the gains are not recommended to be too high for a smooth observation performance. Typically, the observer gain for the q-axis current loop disturbance observer η_q should be tuned relatively larger because q-axis disturbance will change abruptly at load torque sudden change. Also, the observer gain tuning should be done from the inside to the outside because both observers in the q-axis channel are coupled. And a fast enough q-axis current recovery should be guaranteed first before tuning the outer loop speed observer.

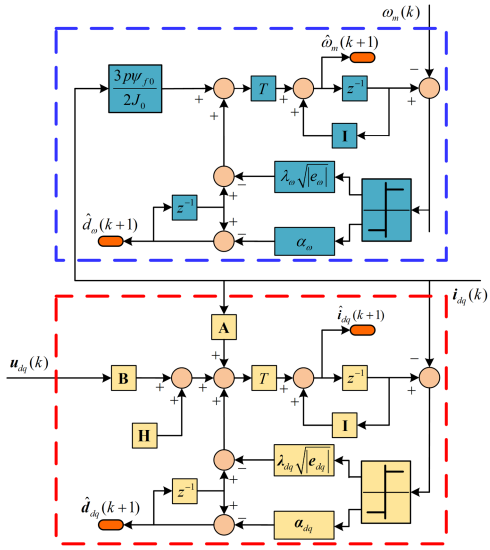

Fig. 2. Block diagram of the proposed dual SOSMDO structure.

The block diagram of the proposed dual SOSMDO structure is displayed in Fig. 2. Obviously, the method decouples the inner and outer disturbance for individual estimation, which means that each observer gain can be specially designed considering different amplitudes and change rates of the inner and outer loop disturbance. Therefore, the best disturbance observation performance can be achieved with the most minor chattering phenomenon. And the proposed RDP-DSC controller can compensate for the overall disturbances completely, and the proposed RDP-DSC method can ensure an ideal deadbeat control behavior even with severe disturbances.

C. Implementation of RDP-DSC

The overall control schematic diagram of the RDP-DSC controller is illustrated in Fig. 3, and the following steps cover the whole digital implementation scenario.

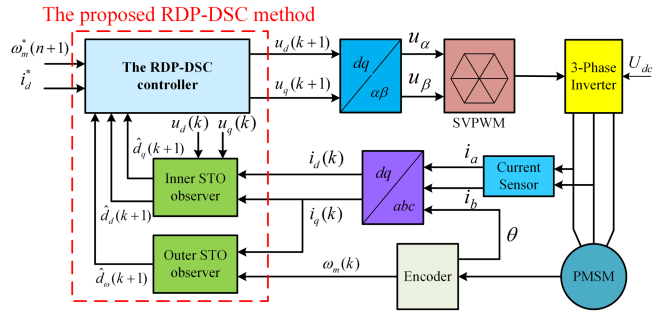

Fig. 3. Schematic diagram of the PMSM control system based on the proposed RDP-DSC method.

1) Disturbance Observation: In the first step, the microprocessor samples all the states at $t = k$, including dq-axis current $\boldsymbol{i}_{dq}(k)$ and the motor speed $\omega_m(k)$. These values then serve as the state feedback to the discretized dual SOSMDO (26) and (27) for estimating current and speed-loop disturbance, respectively. Accordingly, disturbances estimation $\hat{\boldsymbol{d}}_{dq}(k+1)$ and $\hat{d}_\omega(k+1)$ can be obtained

$$\begin{cases} \hat{\boldsymbol{i}}_{dq}(k+1) = \hat{\boldsymbol{i}}_{dq}(k) + T\mathbf{A}(k)\boldsymbol{i}_{dq}(k) + T\mathbf{B}(k)\boldsymbol{u}_{dq}(k) \\ +T\mathbf{H}(k) + T\hat{\boldsymbol{d}}_{dq}(k) - T\boldsymbol{\lambda}_{dq}\sqrt{|\boldsymbol{e}_{dq}(k)|}sign(\boldsymbol{e}_{dq}(k)) \\ \hat{\boldsymbol{d}}_{dq}(k+1) = \hat{\boldsymbol{d}}_{dq}(k) - T\boldsymbol{\alpha}_{dq}sign(\boldsymbol{e}_{dq}(k)) \end{cases} \tag{26}$$

$$\begin{cases} \hat{\omega}_m(k+1) = \hat{\omega}_m(k) - T_p\frac{3p\psi_{f0}i_q(k)}{2J_0} \\ -T_p\lambda_\omega\sqrt{|e_\omega(k)|}sign(e_\omega(k)) + T_p\hat{d}_\omega(k) \\ \hat{d}_\omega(k+1) = \hat{d}_\omega(k) - T_p\alpha_\omega sign(e_\omega(k)). \end{cases} \tag{27}$$

2) One-Step Delay Compensation: Once inner and outer loop disturbances are acquired in the previous step, accurate one-step ahead dq-axis current prediction can be realized. Further, the accurate prediction value $\hat{\boldsymbol{i}}_{dq}(k+1)$ is written as follows, which combines the nominal model prediction value (4) and the observed disturbance at $t = k$:

$$\begin{cases} \hat{i}_d(k+1) = \hat{i}_{d0}(k+1) + T\hat{d}_d(k) \\ \hat{i}_q(k+1) = \hat{i}_{q0}(k+1) + T\hat{d}_q(k). \end{cases} \tag{28}$$

3) RDP-DSC Control Voltage Generation: Considering together disturbance compensation and time delay, the discrete form of the proposed RDP-DSC method can be written as follows, where $u_d(k+1)$ and $u_q(k+1)$ are the final control signals to be implemented to the inverter at time $t = k$:

$$\begin{cases} u_q(k+1) = \frac{L_0}{T}\cdot Sat\left(\frac{2J_0}{3p\psi_{f0}}\left(\frac{-\omega_m(n)+\omega_m^*(n+1)}{T\xi} - \hat{d}_\omega(k)\right)\right) \\ \quad -\frac{L_0}{T}\cdot\left(1-\frac{TR_0}{L_0}\right)\cdot\hat{i}_q(k+1) \\ \quad +(L_0\hat{i}_d(k+1)+\psi_{f0})\omega_e(k) - L_0\hat{d}_q(k+1) \\ u_d(k+1) = \frac{L_0}{T}\cdot i_d^* - \frac{L_0}{T}\left(1-\frac{TR_0}{L_0}\right)\cdot\hat{i}_d(k+1) \\ \quad -\omega_e(k)L_0\hat{i}_q(k+1) - L_0\hat{d}_d(k+1). \end{cases} \tag{29}$$

4) Voltage Constraint: The voltage constraint must be considered before delivering the calculated voltage to the inverter. Thus, the amplitude of the reference voltage should be clamped beforehand by $U_{\rm dc}/\sqrt{3}$, where $U_{\rm dc}$ denotes the dc-link voltage.

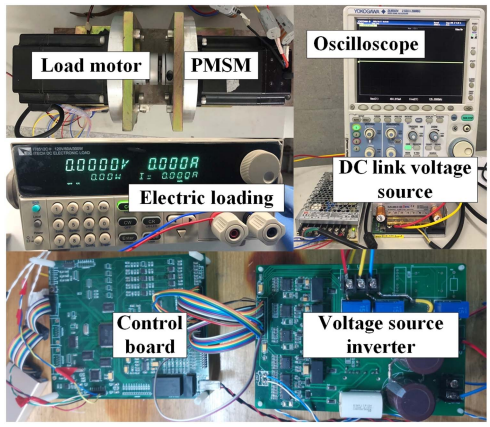

Fig. 4. Actual PMSM experimental platform.

TABLE I
PARAMETERS RELATED TO THE TEST MOTOR

Parameters	Value	Unit
DC-link voltage	120	V
Rated speed	1000	rpm
Pole pairs	5	
Flux linkage	0.059333	Wb
Inertia	0.000325	kg·m²
Inductance	0.0014	H
Resistance	0.72	Ω

If the calculated reference voltage exceeds this limitation, the following scaling method (30) will be adopted. In this case, the results with prime are the final control signal

$$\begin{cases} u'_d(k+1) = \frac{U_{\rm dc}}{\sqrt{3}}\cdot\frac{u_d(k+1)}{\sqrt{u_d(k+1)^2+u_q(k+1)^2}} \\ u'_q(k+1) = \frac{U_{\rm dc}}{\sqrt{3}}\cdot\frac{u_q(k+1)}{\sqrt{u_d(k+1)^2+u_q(k+1)^2}}. \end{cases} \tag{30}$$

V. EXPERIMENTS

Experiments are performed on a digital PMSM system platform based on a TMS320F28335 microprocessor to verify the effectiveness of the proposed RDP-DSC method, as shown in Fig. 4. An SPMSM is used, and both the electrical and mechanical parameters are displayed in Table I. Moreover, the PWM frequency is set as 10 kHz, adding a dead zone of 1 μs. An incremental encoder with 10 000 pulses per revolution is used to measure the actual rotor position of the PMSM, which is fed to eQEP module in the microprocessor for position decoding. Phase A and B currents are measured by the LA100-P transducer before being delivered to the analog-to-digital interface. The sampling rates of speed and current are both set as 10 kHz. Also, $I_{q\max}$ is set as 5 A in the experiment. ξ in the speed control period is set as 10. All the related parameters are appropriately tuned according to the tuning method introduced in Section IV-B for the best observation and control performance. And here symbol "rpm" is used to have the same meaning as "r/min."

For comparison, the conventional DP-DSC method, the DP-DSC method with a sliding-mode torque observer (DP-DSC-TO), and DP-DSC with full parameter disturbances and load torque observer (DP-DSC-FPLO) are also applied. DP-DSC-FPLO has a single observer structure with its detailed procedure listed in [22]. Also, DP-DSC-TO is deliberately created with a dual observer structure for testing the superiority of the proposed SOSMDO. The TO follows the rules in [28], and the integral compensation in [41] is used for the current prediction correction. An "Appendix" briefly introducing both comparison methods with basic formulas and diagrams are given at the end. Meanwhile, the overall calculation time of the proposed RDP-DSC method is about 26.6 μs. The experimental results are given as follows.

A. Steady-State Performance Test

In this section, the steady-state performance under 1000 r/min rated speed operation is evaluated in the case of various parameter mismatches. And the robustness of the proposed RDP-DSC method as well as the sensitivity analysis are experimentally verified.

The steady-state performance of the aforementioned four methods is displayed in Figs. 5–8 under different parameter mismatches when the motor operates at a rated speed of 1000 rpm. The parameter mismatch happens in the middle moment of the figure, and the instant is designated by a straight dashed line. Moreover, the control performance with or without parameter mismatch is evaluated in terms of the current and speed tracking ability as well as the speed fluctuation. Key experimental data are labeled in the waveforms, including dq-axis current, speed ripple, and the steady-state error of the conventional method. And a local enlargement (40 ms/div) is made at transient to reflect the details.

Fig. 5 shows the speed response controlled by different algorithms with 50% inductance error ($L_0 = 1.5L$) at rated speed 1000 r/min. By the conventional DP-DSC method, steady-state tracking errors exist including the speed response tracking error $\Delta\omega_m = -3.8$ rpm, q-axis tracking error $\Delta i_q = 0.15$ A, and d-axis tracking error $\Delta i_d = -0.91$ A. Since the nominal value is 50% larger than the real value, the steady-state tracking performance may have a negative deviation from the reference according to (16), and some underdamping characteristics will occur at transient because of the closed-loop pole at $z = -0.5$. A steady-state tracking error of about -3.8 rpm exists in the experiments, consistent with the analysis. Note that the oscillation at transient is not apparent because the speed change is too tiny. As for the comparison methods, it can be seen that the other three methods can effectively eliminate the steady-state tracking error. However, the proposed RDP-DSC method can ensure the slightest speed ripple of about 3.9 rpm compared with -12.1 rpm in DP-DSC-TO and 4.5 rpm in DP-DSC-FPLO. Hence, RDP-DSC has the best compensation performance under inductance error.

Another group of experimental results in Fig. 6 manifests the motor behavior when flux linkage mismatch suddenly happens. From Fig. 6(b), at the moment of 50% flux linkage ($\psi_{f0} = 1.5\psi_f$)

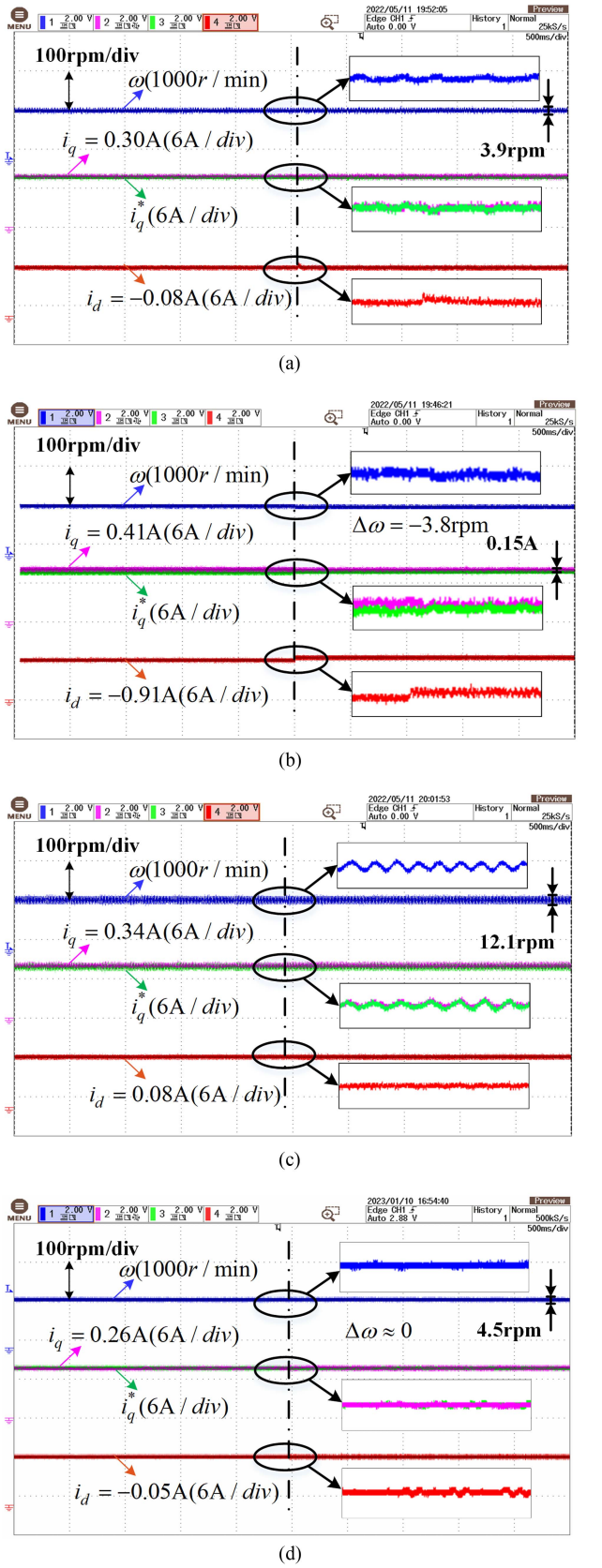

Fig. 5. Experimental results of three different methods under 50% inductance error ($L_0 = 1.5L$) sudden change and 1000 r/min speed. (a) Proposed RDP-DSC method. (b) Conventional DP-DSC method. (c) DP-DSC-TO method. (d) DP-DSC-FPLO method.

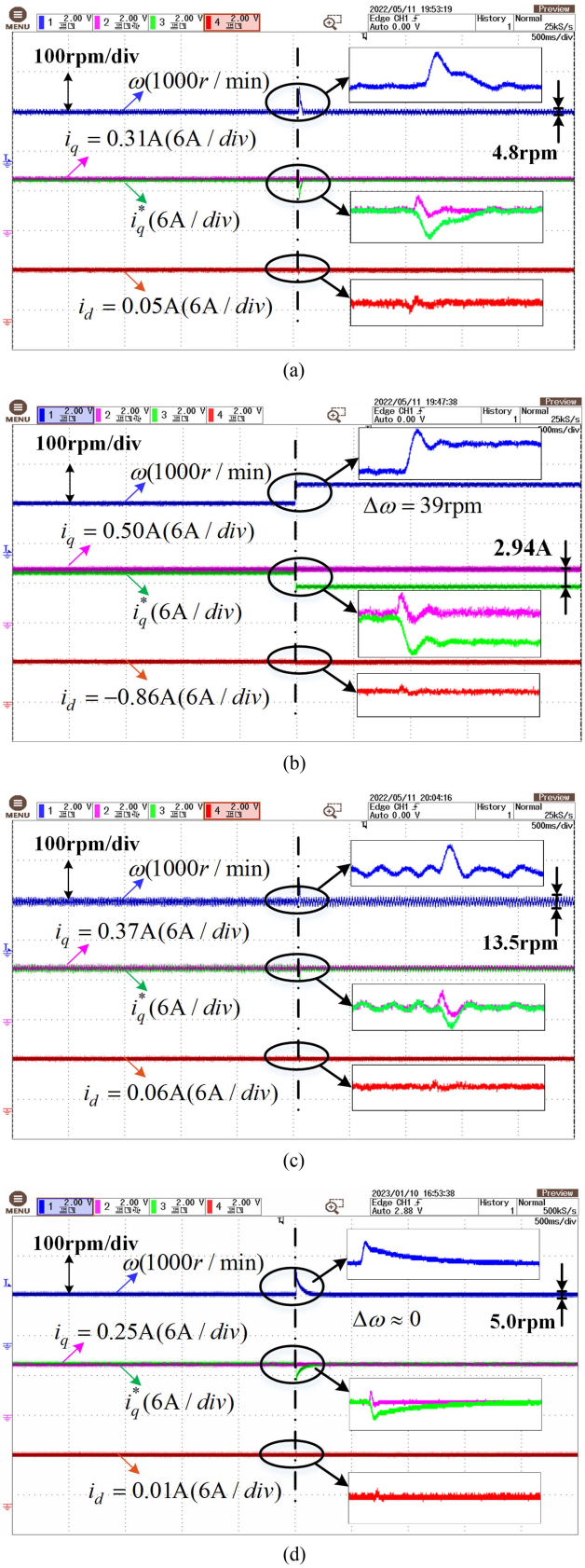

Fig. 6. Experimental results of three different methods under 50% flux linkage error ($\psi_{f0} = 1.5\psi_f$) sudden change and 1000 r/min speed. (a) Proposed RDP-DSC method. (b) Conventional DP-DSC method. (c) DP-DSC-TO method. (d) DP-DSC-FPLO method.

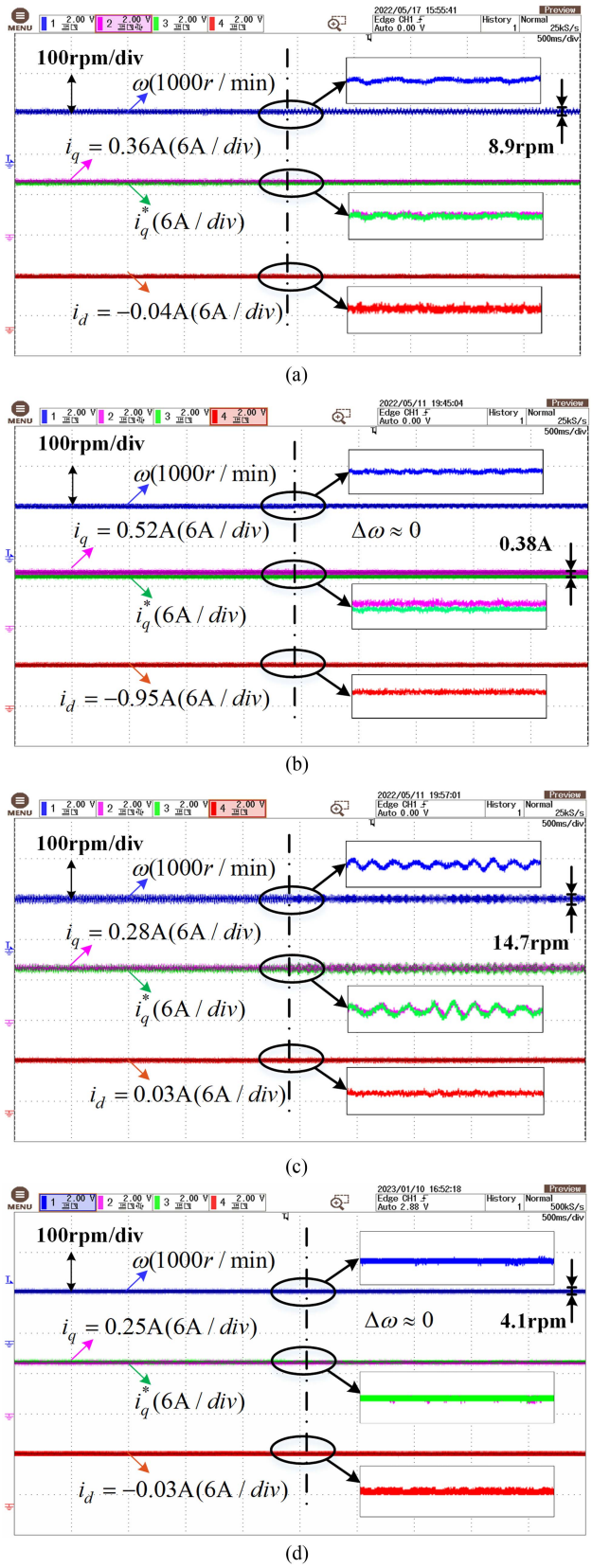

Fig. 7. Experimental results of three different methods under 50% inertia error ($J_0 = 0.5J$) sudden change and 1000 r/min speed. (a) Proposed RDP-DSC method. (b) Conventional DP-DSC method. (c) DP-DSC-TO method. (d) DP-DSC-FPLO method.

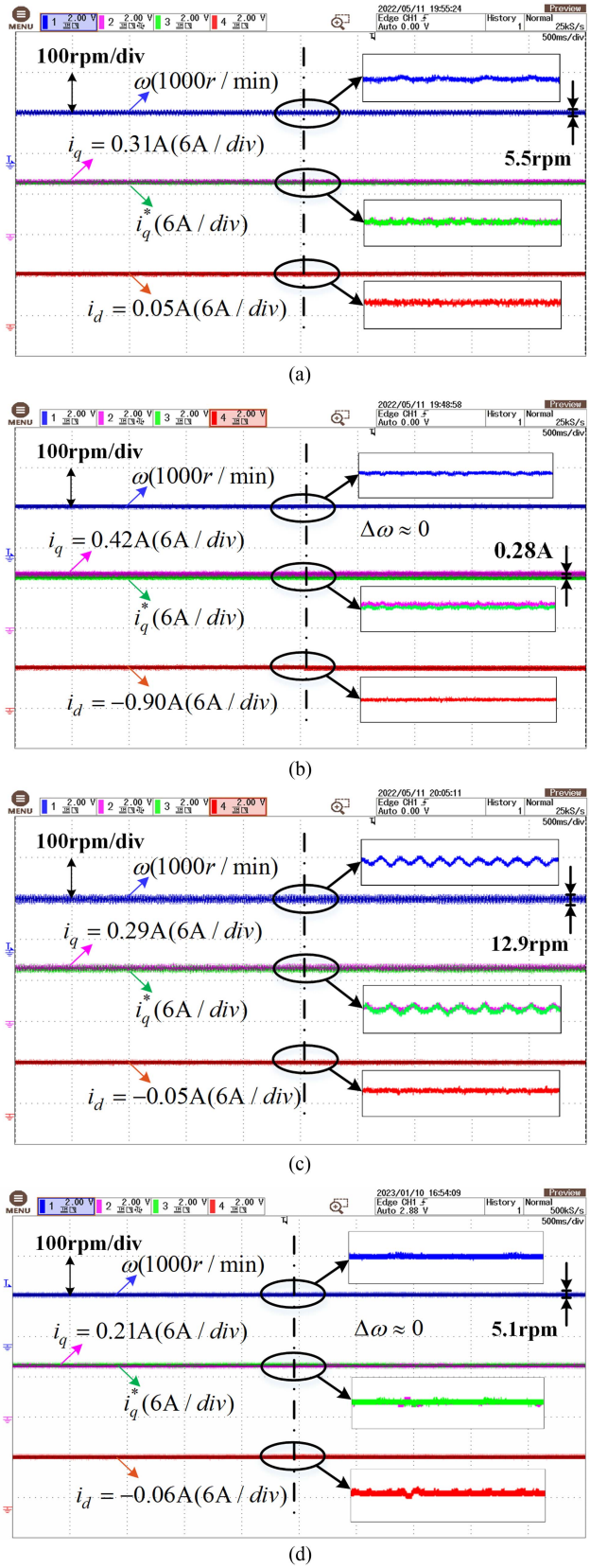

Fig. 8. Experimental results of three different methods under 100% resistance error ($R_0 = 2R$) sudden change and 1000 r/min speed. (a) Proposed RDP-DSC method. (b) Conventional DP-DSC method. (c) DP-DSC-TO method. (d) DP-DSC-FPLO method.

change, significant tracking errors occur both in the speed and q-axis current response, with a value of about 39 rpm and 2.49 A, respectively. This phenomenon is consistent with the sensitivity analysis above, where the predicted speed tracking error will reach about 44 rpm theoretically according to (10) in Section III. In this case, the actual motor speed goes far beyond the reference signal with the conventional DP-DSC method, which means that the flux linkage mismatch will harm the control performance most. Accordingly, it can be calculated that the system is stable because the closed-loop pole at $z = -0.587$ is in the unit circle. Obviously, RDP-DSC (4.8 rpm) and DP-DSC-FPLO (5.0 rpm) have the most minor speed ripple compared with DP-DSC-TO (13.5 rpm). However, the speed recovery time of the proposed method (52.4 ms) is much shorter than DP-DSC-FPLO (202.3 ms), which means RDP-DSC has a better disturbance rejection ability. This phenomenon makes sense because FPLO is still constructed by first-order sliding mode principle. If the observer gains are tuned moderately for less chattering, the disturbance rejection property will be sacrificed. And this contradiction can be successfully avoided by the proposed dual SOSMDO structure in essence. In this case, RDP-DSC holds the best transient performance both at sudden parameter change and at steady-state performance.

Further, the comparison methods' experimental results are shown in Figs. 7 and 8 when the motor inertia mismatch ($J_0 = 0.5J$) and resistance mismatch ($R_0 = 2R$) happen. As shown in Fig. 7(b), a 50% increase in inertia from the actual value has minimal effect on the speed tracking behavior, except for a slight introduction of around 0.38 A tracking error in the q-axis current. Similarly, in Fig. 8(b), the conventional DP-DSC will not exhibit any speed tracking error in 100% resistance bigger case, but the q-axis tracking error still exists. Compared with other parameter differences, the resistance and inertia errors have the least influence on the speed control performance. The experimental results above show the sensitivity analysis's correctness in Section III. Various techniques aiming at dealing with the static errors by certain specially designed observers are experimentally testified in Figs. 7(a), (c), (d) and 8(a), (c), (d). Despite achieving offset-free tracking, DP-DSC-TO exhibits more chattering compared to the other two methods. On the other hand, the proposed RDP-DSC method delivers a satisfactory speed control performance even under conditions of inertia and resistance errors.

As for the effect of inverter nonlinearity, the dead time used in the experiments is 1 μs (100 μs control period), which is a small value with negligible effect on the overall control performance compared to other disturbances, for example, parameter mismatches. The diode and IGBT voltage drops are 1.75 and 1.7 V, respectively, according to the datasheet, which is relatively small compared with the rated voltage of 120 V in the experiments. Hence, it is reasonable to assume that the inverter nonlinearity has little influence on the speed control performance. The left half waveforms can also prove this assumption in Figs. 5 to 8(b), where no parameter mismatches happen. Apparently, there is hardly any tracking error and high-order vibration in the speed response.

In conclusion, all three compensation schemes can achieve deadbeat steady-state tracking performance with the existence of parameter mismatches. The proposed RDP-DSC method as well as the DP-DSC-FPLO have similar speed ripple and chattering, which is much smaller than DP-DSC-TO. However, it can be seen that the disturbance rejection ability of the proposed method is much better than DP-DSC-FPLO because of the novel dual SOSMDO structure.

B. Load Torque Test

In addition to the steady-state error performance comparison under parameter mismatches, the dynamic performance is also evaluated at the sudden change of load torque with and without parameter mismatches in this section. In this scenario, the proposed method can also validate the tracking ability of the q-axis current.

Fig. 9 contains the corresponding motor speed, q-axis current reference (green) and feedback (pink), and the phase-A current from top to bottom under 1000 rpm and 1 N·m torque condition with no parameter error. Moreover, Fig. 10 shows the same condition under 50% inductance error, 50% flux linkage error, 50% inertia error, and 100% resistance error ($L_0 = 1.5L$, $\psi_{f0} = 1.5\psi_f$, $J_0 = 0.5J$, and $R_0 = 2R$). Such an extreme parameter error situation typically does not happen in reality, and the experiments consider extreme cases for robustness testing. In this group of experiments, η_d, η_q, and η_ω are tuned as 50 000, 1200 000, and 64 000, respectively, for the best performance after careful tuning according to the guideline in Section IV. The tracking error of motor speed reaches about -29 rpm after 1 N·m torque is exerted by the conventional DP-DSC, while the theoretical value is -29.38rpm according to (17). This result perfectly proves the correctness of the proposed sensitivity analysis. Also note that the phase current has an amplitude of about 1.4 A under no load case. This phenomenon is reasonable because of the existence of d-axis current tracking error when there is no compensation scheme. Similarly, in Fig. 10(b), the speed steady-state error reaches about 12 rpm below the reference with parameter mismatch and load torque. Such a larger steady-state error is not acceptable in high-quality applications.

In comparison, the other three compensation methods can effectively eliminate speed and dq-axis current tracking errors. Even so, our proposed method seems to have the best performance in terms of speed ripple as well as the transient process. That is, DP-DSC-TO in Figs. 9(c) and 10(c) exhibit about 200 ms severe zig-zag behavior during the transition, while the largest speed fluctuation in the response reaches about 13.9 rpm. As for DP-DSC-FPLO, the chattering reach about 10.2 and 8.1 rpm for both cases while the values for the proposed RDP-DSC are 5.2 and 5.4 rpm, respectively. The behavior of DP-DSC-FPLO becomes worse regarding the speed chattering than the performance in the steady-state test because the disturbance grows at load torque change. So higher observer gains are needed for convergence in this single observer structure. Nevertheless, the disturbance rejection ability is still not as good as the proposed method considering the significant speed fall spike in Fig. 10(d). Therefore, it can be concluded that RDP-DSC shows superiority

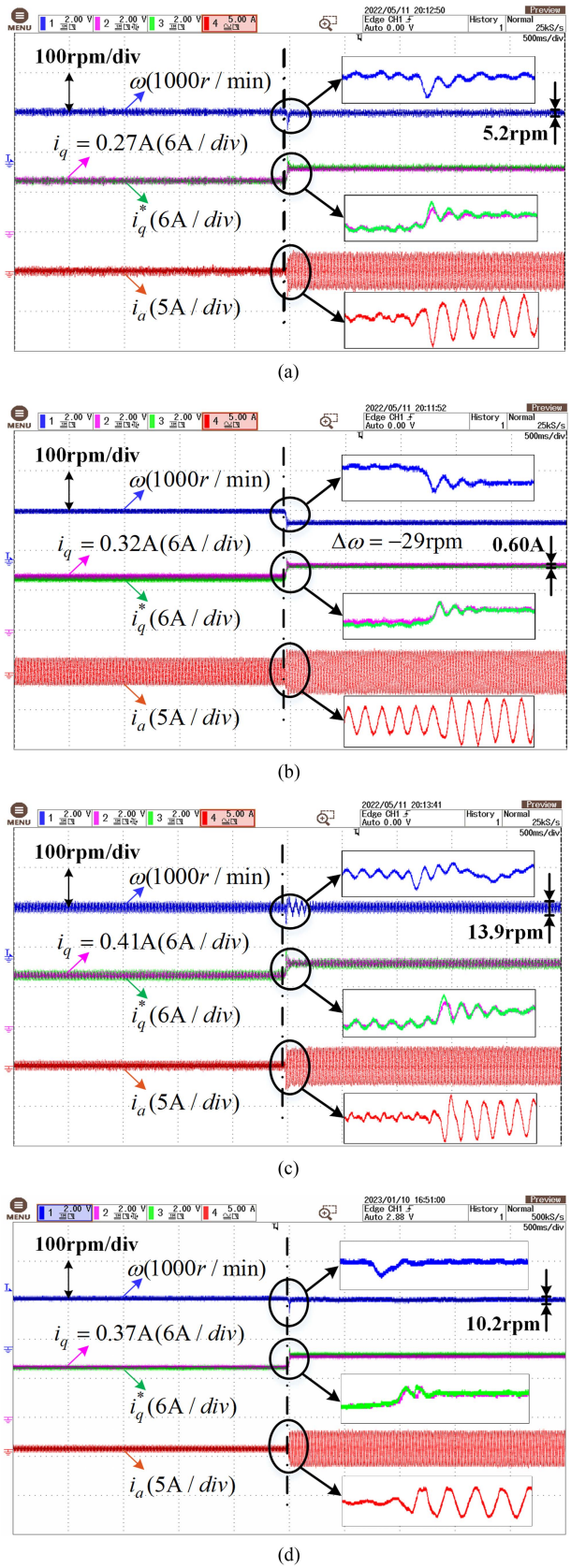

Fig. 9. Experimental results of three different methods under 1 N·m rated load torque step change with no parameter mismatch and 1000 r/min speed. (a) Proposed RDP-DSC method. (b) Conventional DP-DSC method. (c) DP-DSC-TO method. (d) DP-DSC-FPLO method.

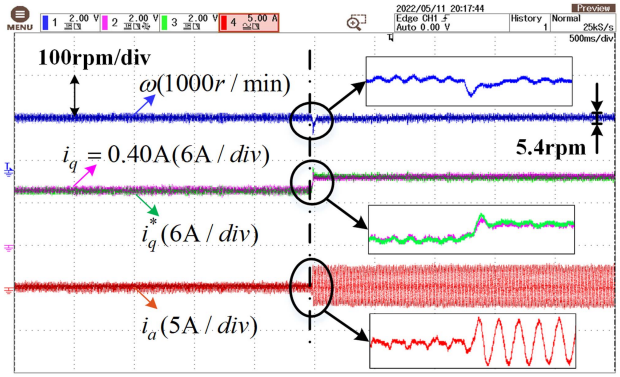

(a)

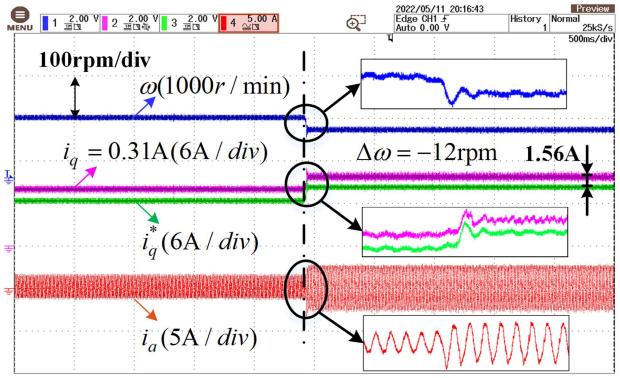

(b)

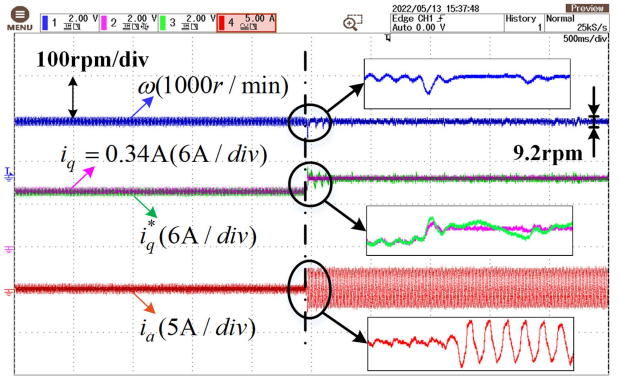

(c)

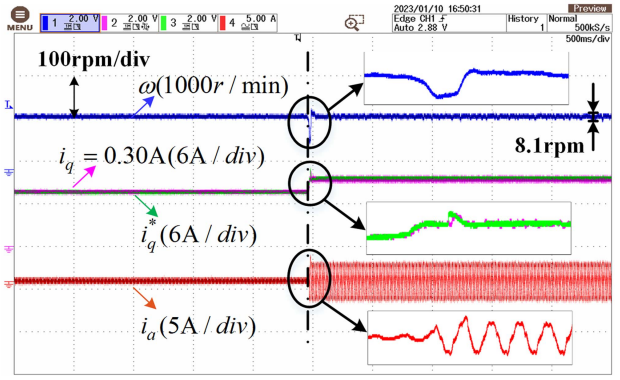

(d)

Fig. 10. Experimental results of three different methods under 1 N·m rated load torque step change with parameter mismatch ($L_0 = 1.5L$, $\psi_{f0} = 1.5\psi_f$, $J_0 = 0.5J$, and $R_0 = 2R$) and 1000 r/min speed. (a) Proposed RDP-DSC method. (b) Conventional DP-DSC method. (c) DP-DSC-TO method. (d) DP-DSC-FPLO method.

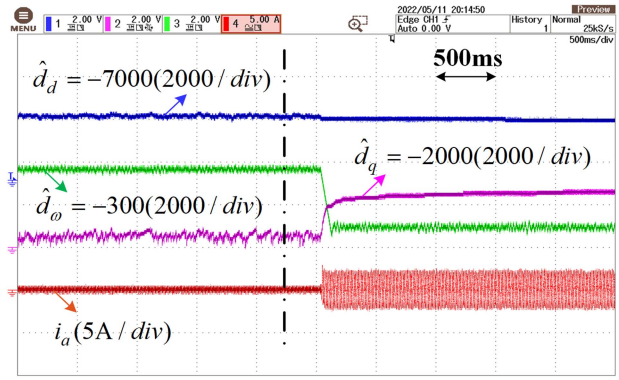

Fig. 11. Experimental results of the observed disturbance value $\hat{d}_d$, $\hat{d}_q$, and $\hat{d}_\omega$ along with the a-phase current at sudden load torque change 1 N·m without parameter mismatches by the proposed RDP-DSC method.

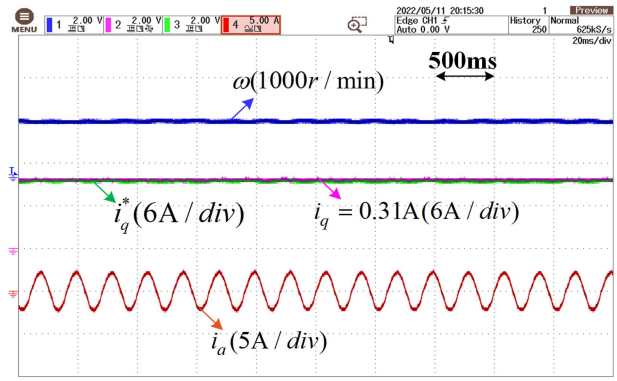

Fig. 12. Experimental results of detailed figure on speed, dq-axis current, and a-phase current control performance by the proposed RDP-DSC method at rated load 1 N·m, rated speed 1000 r/min, and without parameter mismatches.

both in the steady state and in terms of robustness. And the advantages of the proposed dual SOSMDO structure stand out, especially in load case, because of the decoupled dual loop disturbance estimation structure and optimized observer gains.

Meanwhile, another group of experiments is designed to visualize the observed speed and current loop disturbance in detail by our designed SOSMDO when there is no parameter mismatch. The load torque is exerted in the middle and the change of the estimated disturbances is clearly illustrated in Fig. 11. From the result, the sudden change of the estimated inner q-axis current loop disturbance $\hat{d}_q$ and outer speed loop disturbance $\hat{d}_\omega$ shows the effect of load torque on the system. The d-axis current disturbance $\hat{d}_d$ hardly changes, which is reasonable because the torque dynamics are decoupled from the d-axis. Meanwhile, these observed values are used for compensation to achieve deadbeat speed control performance. Since the definition of these disturbances is some specific physical values (current or voltage) over corresponding constants (torque factor or inductance) according to (1), the physical meaning is not the main focus, and hence the unit is set to null in the figure. What is more, Fig. 12 displays the detailed figure under nominal speed and load torque operating case. The conclusion that the proposed RDP-DSC method can achieve good speed control

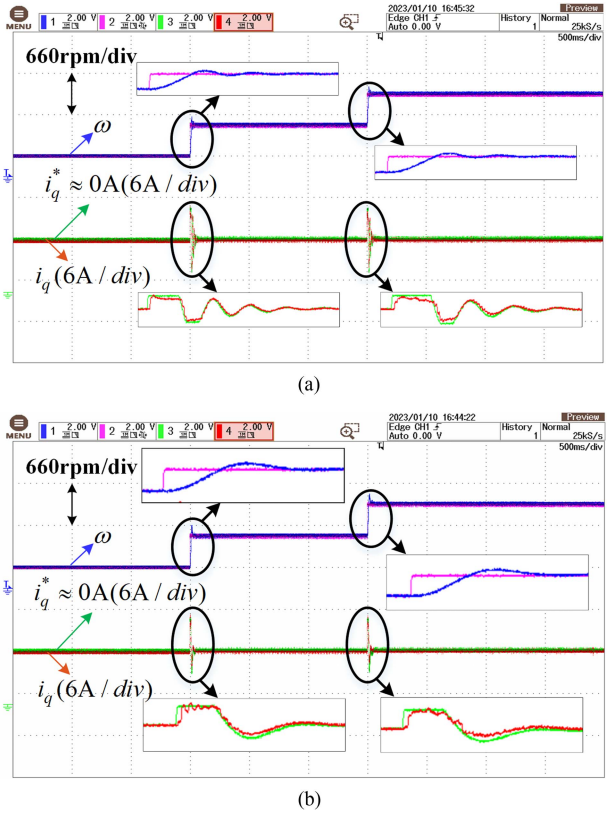

Fig. 13. Speed step response of the proposed RDP-DSC method from 0 to 500 to 1000 rpm. (a) Without parameter mismatch. (b) With parameter mismatch ($L_0 = 1.5L$, $\psi_{f0} = 1.5\psi_f$, $J_0 = 0.5J$, and $R_0 = 2R$).

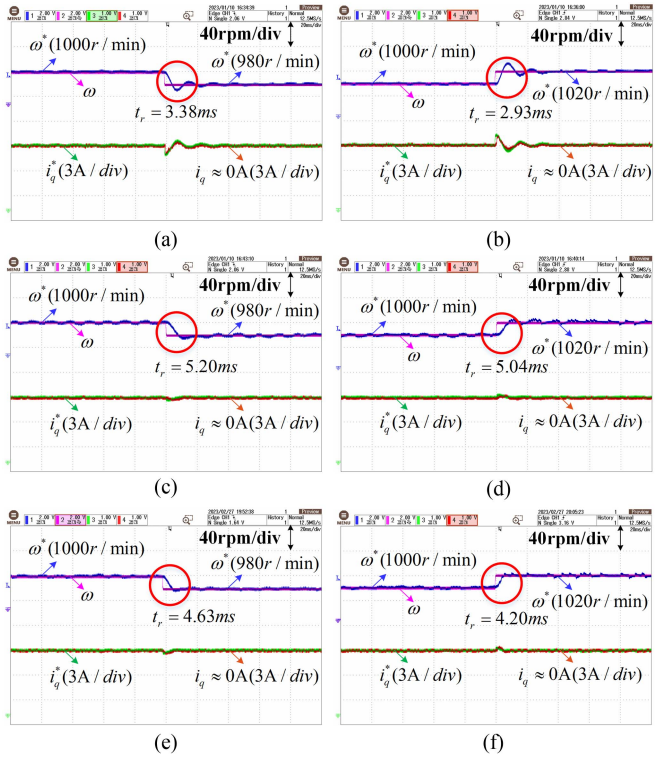

Fig. 14. Bandwidth test experimental results of 20 rpm (2% rated) speed step reference without torque saturation. (a) Proposed RDP-DSC method under 1000 to 980 rpm reference. (b) Proposed RDP-DSC method under 1000 to 1020 rpm reference. (c) Cascaded PI method under 1000 to 980 rpm reference. (d) Cascaded PI method under 1000 to 1020 rpm reference. (e) Cascaded PFC-PCC method under 1000 to 980 rpm reference. (f) Cascaded PFC-PCC method under 1000 to 1020 rpm reference.

performance without steady-state error can be drawn from the perfect sinusoidal phase current profile.

C. Dynamic Performance Test

The improvement of dynamics is one of the critical advantages of DSC compared with conventional cascaded structure. This section conducts two sets of experiments for dynamical performance evaluation, that is, the speed step response test and bandwidth test.

Firstly, speed step tests are performed with the speed reference starting from 0 to 500 to 1000 rpm covering the situation of both without parameter mismatch case and with parameter mismatch case ($L_0 = 1.5L$, $\psi_{f0} = 1.5\psi_f$, $J_0 = 0.5J$, and $R_0 = 2R$). The results are given in Fig. 13, and both figures verify that the deadbeat speed control performance can be achieved without any steady-state error. As for the transient performance, the settling time is about 11.08 ms in Fig. 13(a), while 11.88 ms in Fig. 13(b). It can be concluded that the RDP-DSC method can guarantee satisfying dynamic speed tracking performance even under strong parameter mismatches, which means that the RDP-DSC method can add robustness without impairing the tracking ability. And the experiments prove the feasibility and effectiveness of the proposed method.

Further, the authors test the bandwidth improvement of the cascaded-free structure in the proposed method under small speed reference. In fact, the bandwidth of the whole system can be evaluated by the term called "practical bandwidth" from the control theory field [20]. That is, the system's bandwidth $f_{\rm bw}$ can be approximated by the 10%–90% rise time t_r from (31) according to [42]. Hence, the authors perform experiments comparing the speed response bandwidth of the proposed RDP-DSC method with the conventional cascaded PI controller. The speed step reference is scaled to avoid torque saturation, and the amplitude is set as 20 rpm (2% rated value) in the experiments

$$f_{\rm bw} = \frac{0.35}{t_r}. \tag{31}$$

Fig. 14 shows the results in the bandwidth test with 20 rpm speed step tracking response where (a), (c), and (e) are the cases under 1000 to 980 rpm speed reference using the proposed RDP-DSC method, cascaded PI control, and cascaded PFC-PCC method, respectively. The PFC-PCC method adopts full predictive controller for both speed and current loops, which uses the robust PCC from [29] for current control and predictive functional control method in [43] for speed control. The full predictive cascaded control method is designed to better illustrate the proposed cascaded-free RDP-DSC method's superiority over other cascaded methods. On the contrary, (b), (d), and (f) show the cases when the speed reference jumps from 1000 to 1020 rpm with the three methods. From the results, it can be observed that the average rise time of RDP-DSC is about 3.15 ms, and the corresponding bandwidth is 111.1 Hz.

In comparison, the rise time of the cascaded PI controller is about 5.12 ms, while the bandwidth is about 68.4 Hz. And the bandwidth of cascaded PFC-PCC is about 79.3 Hz with a 4.42 ms rise time. Obviously, the proposed RDP-DSC has a significant improvement in bandwidth than the other conventional cascaded controller structure, which means that much better dynamics can be achieved. Another point to note is that the PI controller's coefficients have already been tuned relatively large for faster transient performance. Even so, the response speed is much slower while the speed response graphs in (c) and (d) exhibit larger ripple compared to the proposed RDP-DSC method. Also, even if the cascaded full predictive method has a slightly smoother response, it scarifies a lot on the dynamics speed, which is not desirable in high-end drives. In conclusion, the bandwidth test proves that the proposed RDP-DSC method significantly outperforms other cascaded control methods in terms of fast dynamics. And perfect deadbeat speed tracking can be achieved under small speed step reference by the proposed method.

VI. Conclusion

A novel RDP-DSC method for high-quality PMSM speed control is put forward in this article. The main contributions include 1) sensitivity analysis on how parameter mismatches, external disturbances and inverter nonlinearity affect the speed tracking performance is quantitatively performed; and 2) a novel dual SOSMDO structure with multiple advanced observers are designed for separately compensating the inner and outer loop disturbance. The gains can be specially tuned considering different disturbance features for the best observation and control performance.

Both the sensitivity analysis and feasibility of the proposed RDP-DSC method are experimentally verified. The results show that the RDP-DSC method has superiority over other conventional SMO-based compensation DSC methods in terms of lower speed ripple and stronger disturbance rejection ability. Meanwhile, the significant bandwidth improvement of the proposed method is also proved compared with the conventional cascaded structure. Future work may include extending the RDP-DSC method to interior PMSM and field weakening working conditions.

Appendix

This section briefly introduces the comparison methods, that is, DP-DSC-TO and DP-DSC-FPLO, including their basic formulas and block diagrams. This part is a supplementary to the experiment section for better comparison and verification of the proposed method's superiority.

A. DP-DSC-FPLO Method

The DP-DSC-FPLO method in [22] adopts a sliding-mode FPLO method to simultaneously estimate electrical parameter disturbances, mechanical parameter disturbances, motor speed, and load torque. This method uses a single SMO to estimate the overall lumped disturbance in DSC topology. The control signal

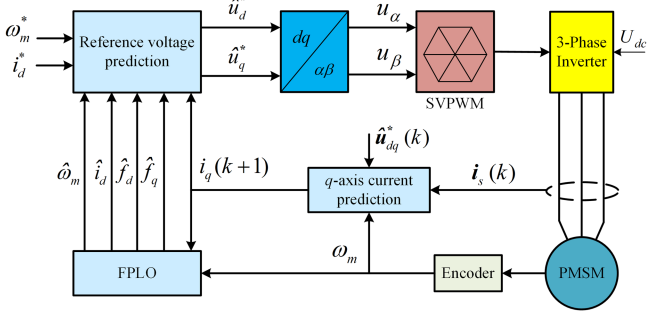

Fig. 15. Block diagram of the PMSM system based on DP-DSC-FPLO method.

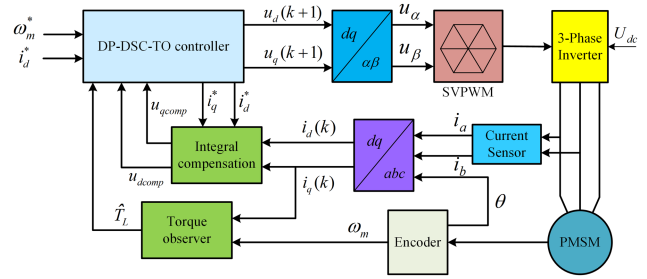

Fig. 16. Block diagram of the PMSM system based on DP-DSC-TO method.

of DP-DSC-FPLO can be written in the following form:

$$\hat{\boldsymbol{u}}^*_{dq} = \begin{bmatrix} \hat{u}^*_d \\ \hat{u}^*_q \end{bmatrix} = \begin{bmatrix} \frac{L}{T_s}\cdot i^*_d + \hat{a}(k+1) + \hat{f}_d(k+1) \\ \frac{L}{T_s}\cdot \frac{2J(\omega^*-\hat{\omega}(t))+2T_{sp}pT_l}{3p^2\psi_f T_{sp}} + \hat{b}(k+1) + \hat{f}_q(k+1) \end{bmatrix} \tag{32}$$

where $\hat{f}_q(k+1)$ and $\hat{f}_d(k+1)$ are the output of FPLO; $\hat{a}(k+1)$ and $\hat{b}(k+1)$ are intermediate variables calculated by the current, speed, and motor parameters.

The block diagram of DP-DSC-FPLO is shown as Fig. 15. First, the sampled current $\boldsymbol{i}_s(k)$ and the control signal $\hat{\boldsymbol{u}}^*_{dq}(k)$ at $t = k$ are used to predict the q-axis current $i_q(k+1)$ for $t = k+1$ because of the delay compensation issue. Further, FPLO is adopted to acquire the disturbance estimation $\hat{f}_q$ and $\hat{f}_d$, the d-axis current estimation $\hat{i}_d$, and the speed estimation $\hat{\omega}_m$. Finally, all the outputs from FPLO are fed into the controller for the final control signal $\hat{\boldsymbol{u}}^*_{dq}$ generation (32), which is then delivered to the inverter for DP-DSC-FPLO realization.

B. DP-DSC-TO Method

DP-DSC-TO method combines a sliding-mode load TO from [28] and an integral current disturbance compensation strategy from [41]. Actually, this combination is deliberately created based on the dual disturbance observer structure with known techniques so that the superiority of the SOMODO observer can be proved. The block diagram of DP-DSC-TO can be depicted by Fig. 16, where $u_{q\mathrm{comp}}$ and $u_{d\mathrm{comp}}$ mean the current loop disturbance calculated by an integral compensation module. A TO estimates the load torque $\hat{T}_L$ so that the speed disturbance can

be considered and eliminated when generating the intermediate current. Finally, the calculated values $u_{q\mathrm{comp}}$, $u_{d\mathrm{comp}}$ and $\hat{T}_L$ are delivered to the DP-DSC-TO controller for offset-free speed control. Both schemes are briefly illustrated as follows.

The load TO is constructed based on (33a), where $e_1 = \hat{\omega}_m - \omega_m$ and $e_2 = \hat{T}_L - T_e$ denote the speed and load torque estimation error, respectively. Meanwhile, all the parameters, such as observer gains g and K, are tuned appropriately in the experiments

$$\begin{cases} \frac{de_1}{dt} = -\frac{p}{J}e_2 + U \\ \frac{de_2}{dt} = g \cdot U \\ U = K \cdot \mathrm{sgn}(e_1). \end{cases} \tag{33a}$$

Besides, the integral current loop disturbance compensation method is a model-independent method that adds the integral of the dq-axis current tracking error to the voltage reference. The formula for calculation $u_{q\mathrm{comp}}$ and $u_{d\mathrm{comp}}$ goes as (33b). And the convergence property and effectiveness of the integral compensation have been mathematically proved in literature

$$\begin{cases} u_{d\mathrm{comp}} = \sum (i_d - i_d^*) \\ u_{q\mathrm{comp}} = \sum (i_q - i_q^*). \end{cases} \tag{33b}$$

REFERENCES

[1] X. Zhang, Y. Cheng, Z. Zhao, and K. Yan, "Optimized model predictive control with dead-time voltage vector for PMSM drives," *IEEE Trans. Power Electron.*, vol. 36, no. 3, pp. 3149–3158, Mar. 2021.

[2] S.-C. Carpiuc and C. Lazar, "Real-time multi-rate predictive cascade speed control of synchronous machines in automotive electrical traction drives," *IEEE Trans. Ind. Electron.*, vol. 63, no. 8, pp. 5133–5142, Aug. 2016.

[3] M. Siami, D. A. Khaburi, A. Abbaszadeh, and J. Rodríguez, "Robustness improvement of predictive current control using prediction error correction for permanent-magnet synchronous machines," *IEEE Trans. Ind. Electron.*, vol. 63, no. 6, pp. 3458–3466, Jun. 2016.

[4] Z. Wang, A. Yu, X. Li, G. Zhang, and C. Xia, "A novel current predictive control based on fuzzy algorithm for PMSM," *IEEE Trans. Emerg. Sel. Topics Power Electron.*, vol. 7, no. 2, pp. 990–1001, Jun. 2019.

[5] P. Acuna, R. P. Aguilera, A. M. Y. M. Ghias, M. Rivera, C. R. Baier, and V. G. Agelidis, "Cascade-free model predictive control for single-phase grid-connected power converters," *IEEE Trans. Ind. Electron.*, vol. 64, no. 1, pp. 285–294, Jan. 2017.

[6] E. Fuentes, D. Kalise, J. Rodríguez, and R. M. Kennel, "Cascade-free predictive speed control for electrical drives," *IEEE Trans. Ind. Electron.*, vol. 61, no. 5, pp. 2176–2184, May 2014.

[7] X. Gao, M. Abdelrahem, C. M. Hackl, Z. Zhang, and R. Kennel, "Direct predictive speed control with a sliding manifold term for PMSM drives," *IEEE J. Emerg. Sel. Topics Power Electron.*, vol. 8, no. 2, pp. 1258–1267, Jun. 2020.

[8] E. J. Fuentes, C. A. Silva, and J. I. Yuz, "Predictive speed control of a two-mass system driven by a permanent magnet synchronous motor," *IEEE Trans. Ind. Electron.*, vol. 59, no. 7, pp. 2840–2848, Jul. 2012.

[9] B. Guo, C. Xia, and J.-F. Han, "NN-based model predictive direct speed control of PMSM drive systems," in *Proc. Int. Conf. Mach. Learn. Cybern.*, 2014, pp. 163–168.

[10] J. Rodriguez et al., "Latest advances of model predictive control in electrical drives—Part II: Applications and benchmarking with classical control methods," *IEEE Trans. Power Electron.*, vol. 37, no. 5, pp. 5047–5061, May 2022.

[11] X. Liu, J. Wang, X. Gao, W. Tian, L. Zhou, and R. Kennel, "Robust predictive speed control of SPMSM drives with algebraically designed weighting factors," *IEEE Trans. Power Electron.*, vol. 37, no. 12, pp. 14434–14446, Dec. 2022.

[12] S. Bolognani, S. Bolognani, L. Peretti, and M. Zigliotto, "Design and implementation of model predictive control for electrical motor drives," *IEEE Trans. Ind. Electron.*, vol. 56, no. 6, pp. 1925–1936, Jun. 2009.

[13] X. Liu et al., "Continuous control set predictive speed control of SPMSM drives with short prediction horizon," *IEEE Trans. Power Electron.*, vol. 37, no. 9, pp. 10166–10177, Sep. 2022.

[14] J. Rodriguez et al., "Latest advances of model predictive control in electrical drives—Part I: Basic concepts and advanced strategies," *IEEE Trans. Power Electron.*, vol. 37, no. 4, pp. 3927–3942, Apr. 2022.

[15] Y. Yao, Y. Huang, F. Peng, J. Dong, and H. Zhang, "An improved deadbeat predictive current control with online parameter identification for surface-mounted PMSMs," *IEEE Trans. Ind. Electron.*, vol. 67, no. 12, pp. 10145–10155, Dec. 2020.

[16] H. T. Nguyen and J.-W. Jung, "Finite control set model predictive control to guarantee stability and robustness for surface-mounted PM synchronous motors," *IEEE Trans. Ind. Electron.*, vol. 65, no. 11, pp. 8510–8519, Nov. 2018.

[17] X. Zhang, L. Zhang, and Y. Zhang, "Model predictive current control for PMSM drives with parameter robustness improvement," *IEEE Trans. Power Electron.*, vol. 34, no. 2, pp. 1645–1657, Feb. 2019.

[18] L. Wang, *Model Predictive Control System Design and Implementation Using MATLAB*. Berlin, Germany: Springer, 2009.

[19] M. Yang, X. Lang, J. Long, and D. Xu, "Flux immunity robust predictive current control with incremental model and extended state observer for PMSM drive," *IEEE Trans. Power Electron.*, vol. 32, no. 12, pp. 9267–9279, Dec. 2017.

[20] M. Preindl and S. Bolognani, "Model predictive direct speed control with finite control set of PMSM drive systems," *IEEE Trans. Power Electron.*, vol. 28, no. 2, pp. 1007–1015, Feb. 2013.

[21] R. Yang, M. Wang, L. Li, G. Wang, and C. Zhong, "Robust predictive current control of PMLSM with extended state modeling based Kalman filter: For time-varying disturbance rejection," *IEEE Trans. Power Electron.*, vol. 35, no. 2, pp. 2208–2221, Feb. 2020.

[22] X. Zhang, Y. Cheng, Z. Zhao, and Y. He, "Robust model predictive direct speed control for SPMSM drives based on full parameter disturbances and load observer," *IEEE Trans. Power Electron.*, vol. 35, no. 8, pp. 8361–8373, Aug. 2020.

[23] Z. Li, F. Wang, D. Ke, J. Li, and W. Zhang, "Robust continuous model predictive speed and current control for PMSM with adaptive integral sliding-mode approach," *IEEE Trans. Power Electron.*, vol. 36, no. 12, pp. 14398–14408, Dec. 2021.

[24] B. Wang, Z. Dong, Y. Yu, G. Wang, and D. Xu, "Static-errorless deadbeat predictive current control using second-order sliding-mode disturbance observer for induction machine drives," *IEEE Trans. Power Electron.*, vol. 33, no. 3, pp. 2395–2403, Mar. 2018.

[25] R. Yang, M. Wang, L. Li, Y. Zenggu, and J. Jiang, "Integrated uncertainty/disturbance compensation with second-order sliding-mode observer for PMLSM-driven motion stage," *IEEE Trans. Power Electron.*, vol. 34, no. 3, pp. 2597–2607, Mar. 2019.

[26] Y. Xu, S. Li, and J. Zou, "Integral sliding mode control based deadbeat predictive current control for PMSM drives with disturbance rejection," *IEEE Trans. Power Electron.*, vol. 37, no. 3, pp. 2845–2856, Mar. 2022.

[27] P. G. Carlet, A. Favato, S. Bolognani, and F. Dörfler, "Data-driven continuous-set predictive current control for synchronous motor drives," *IEEE Trans. Power Electron.*, vol. 37, no. 6, pp. 6637–6646, Jun. 2022.

[28] X. Zhang and Y. He, "Direct voltage-selection based model predictive direct speed control for PMSM drives without weighting factor," *IEEE Trans. Power Electron.*, vol. 34, no. 8, pp. 7838–7851, Aug. 2019.

[29] J. Gao, S. Li, Y. Xu, and J. Zou, "Time-delay compensation method in PMSM servo system based on predictive current control with sensitivity analysis," in *Proc. 22nd Int. Conf. Elect. Mach. Syst.*, 2019, pp. 1–6.

[30] V. Utkin, J. Guldner, and J. Shi, *Sliding Mode Control in Electro-Mechanical Systems*, 2nd ed. Boca Raton, FL, USA: CRC Press, 2009.

[31] Y. Shtessel, C. Edwards, L. Fridman, and A. Levant, *Sliding Mode Control and Observation*, 1st ed. Cambridge, MA, USA: Birkhaüser, Nov. 2014.

[32] H.-J. Ahn and D.-M. Lee, "A new bumpless rotor-flux position estimation scheme for vector-controlled washing machine," *IEEE Trans. Ind. Inform.*, vol. 12, no. 2, pp. 466–473, Apr. 2016.

[33] J. A. Moreno and M. Osorio, "Strict Lyapunov functions for the super-twisting algorithm," *IEEE Trans. Autom. Control*, vol. 57, no. 4, pp. 1035–1040, Apr. 2012.

[34] S. Liu, Q. Wang, G. Zhang, G. Wang, and D. Xu, "Online temperature identification strategy for position sensorless PMSM drives with position error adaptive compensation," *IEEE Trans. Power Electron.*, vol. 37, no. 7, pp. 8502–8512, Jul. 2022.

[35] Y. Wang, Y. Zhu, X. Zhang, B. Tian, K. Wang, and J. Liang, "Antidisturbance sliding mode-based deadbeat direct torque control for PMSM speed regulation system," *IEEE Trans. Transp. Electrific.*, vol. 7, no. 4, pp. 2705–2714, Dec. 2021.

[36] A. U. Rehman, B. A. Basit, H. H. Choi, and J.-W. Jung, "Computationally efficient deadbeat direct torque control considering speed dynamics for a surface-mounted PMSM drive," *IEEE/ASME Trans. Mechatron.*, vol. 27, no. 5, pp. 3407–3418, Oct. 2022.
[37] F. Wang, D. Ke, X. Yu, and D. Huang, "Enhanced predictive model based deadbeat control for PMSM drives using exponential extended state observer," *IEEE Trans. Ind. Electron.*, vol. 69, no. 3, pp. 2357–2369, Mar. 2022.
[38] Y. Jiang, W. Xu, C. Mu, and Y. Liu, "Improved deadbeat predictive current control combined sliding mode strategy for PMSM drive system," *IEEE Trans. Veh. Technol.*, vol. 67, no. 1, pp. 251–263, Jan. 2018.
[39] Y. Wang, Y. Xu, and J. Zou, "Sliding-mode sensorless control of PMSM with inverter nonlinearity compensation," *IEEE Trans. Power Electron.*, vol. 34, no. 10, pp. 10206–10220, Oct. 2019.
[40] S.-H. Hwang and J.-M. Kim, "Dead time compensation method for voltage-fed PWM inverter," *IEEE Trans. Energy Convers.*, vol. 25, no. 1, pp. 1–10, Mar. 2010.
[41] T. Türker, U. Buyukkeles, and A. F. Bakan, "A robust predictive current controller for PMSM drives," *IEEE Trans. Ind. Electron.*, vol. 63, no. 6, pp. 3906–3914, Jun. 2016.
[42] W. S. Levine, *The Control Handbook*. Boca Raton: FL, USA: CRC Press, 1996.
[43] H. Liu and S. Li, "Speed control for PMSM servo system using predictive functional control and extended state observer," *IEEE Trans. Ind. Electron.*, vol. 59, no. 2, pp. 1171–1183, Feb. 2012.

Shaobin Li was born in Liaoning Province, China, in 1997. He received the B.S degree in electrical engineering from the Harbin Institute of Technology (HIT), Harbin, China, in 2019. He is currently working toward the Ph.D degree in electrical engineering with the School of Electrical Engineering and Automation, HIT.

His research interests include permanent magnet motor drives and control.

Yongxiang Xu (Member, IEEE) received the M.S. and Ph.D. degrees in electrical engineering from the Harbin Institute of Technology, Harbin, China, in 2001 and 2005, respectively.

In 2005, he joined the Department of Electrical Engineering, Harbin Institute of Technology, as an Assistant Professor. Since 2013, he has been a Professor with the Department of Electrical Engineering, Harbin Institute of Technology. His research interests include permanent-magnet machine design and control.

Wentao Zhang was born in Shandong Province, China, in 1993. He received the B.S. degree in electrical engineering and automation from the Harbin Institute of Technology, Weihai, China, in 2016, and the Ph.D. degree in electrical engineering from the Harbin Institute of Technology, Harbin, China, in 2021.

He is currently a Lecturer with the Special Motor Research Center, Harbin Institute of Technology, Harbin, China. His research interests include PMSM drives and control algorithms.

Jibin Zou (Senior Member, IEEE) received the M.S. and Ph.D. degrees in electrical engineering from the Harbin Institute of Technology, Harbin, China, in 1984 and 1988, respectively.

Since 1985, he has been engaged in the research in electrical machines. He was with the University of Liverpool, Liverpool, U.K. as a Visiting Research Fellow for 1 year. He is currently a Professor with the State Key Laboratory of Robotics and System, Harbin Institute of Technology.

Dr. Zou has a senior member of the IEEE Magnetics society, since 2000. His research interests include permanent magnet machine design and control.